Modeling Transient Flow in Intermittent Water Supply System

by

Xin Zhang

B.S., Tsinghua University (2015)

Submitted to the Department of Civil and Environmental Engineering
in partial fulfillment of the requirements for the degree of

Master of Science in Civil and Environmental Engineering

at the

MASSACHUSETTS INSTITUTE OF TECHNOLOGY

June 2017

Signature redacted

Author . . . .
Department of Civil and Environmental Engineering
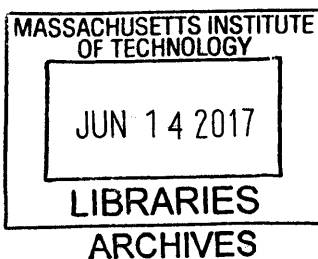May 15, 2017

Signature redacted

Certified by. . . . .
Andrew J. Whittle
Professor of Civil and Environmental Engineering
Thesis Supervisor

Signature redacted

Accepted by . . . .
Jesse Kroll
Professor of Civil and Environmental Engineering
Chair, Graduate Program Committee

Modeling Transient Flow in Intermittent Water Supply System

by

Xin Zhang

Submitted to the Department of Civil and Environmental Engineering
on May 15, 2017, in partial fulfillment of the
requirements for the degree of
Master of Science in Civil and Environmental Engineering

Abstract

Water distribution systems in cities throughout South Asia (and many other countries) only supply water on an intermittent basis (currently averaging less than 5hrs/day in most Indian cities). Intermittent Water Supply (IWS) creates inequities in water availability and carries public health risks associated with the ingress of contaminants from the surrounding ground through flaws in the aged piping systems. It is a major challenge to upgrade from intermittent to continuous water supply (CWS) as this involves an increase in the operating water pressures which promotes higher rates of leakage. There are currently no reliable computational models for characterizing the transient hydraulic behavior of IWS systems (including pipe filling and draining events) and hence, it is difficult to understand and control IWS systems. In a recent PhD thesis, Lieb (2015) developed an open-source code to solve the dynamics of IWS pipe networks through finite volume solution of the governing 1-D Saint Venant equations using the Preismann slot approximation. The current thesis extends and refines the algorithms proposed by Lieb to enable more robust simulations for pipe networks. Specific modification include algorithms for dry pipes and three-pipe junctions. The thesis proposes a new algorithm for representing the conservation of fluid mass, momentum and energy at a three-pipe junction which is validated by comparing computed loss coefficients with measured data reported in the literature. The research also validates predictions of mixed flow conditions (open-channel and pressured pipe flow conditions) with results from laboratory model tests. The proposed formulation has been applied to simulate a skeletonized pipe network (at a test site in Delhi), where simulations are compared with water pressures during intermittent water supply periods. The proposed analysis represents a first step towards comprehensive modeling of IWS that can be used to improve understanding and control of these systems and to manage the upgrading process for CWS operations.

Thesis Supervisor: Andrew J. Whittle
Title: Professor of Civil and Environmental Engineering

Acknowledgments

Contents

8

List of Figures

9

List of Tables

Chapter 1

Introduction

In the US, Europe, China, and much of the developed world, water is supplied on a continuous basis (24-7) through pressurized water distribution pipe networks. However, of the 3.7 billion people with piped water supply, 1 billion have intermittent water supply including 280 million people in cities across India [54]. In more than 45 countries, including all major urban areas in the India sub-continent, IWS systems typically provide water for limited supply periods and either drain or remain at low pressures in the stagnation periods. Figure 1-1 describes a basic situation of IWS in the world, and it can be seen that IWS is widespread in developing countries. Current Indian cities typically average only 4.5 hours of supply per day, shown in Figure 1-2. For example, in Jamshedpur, India, water is supplied to local residents only 4 hours a day: two hours in the morning and another two hours in the evening. In the other 20 hours, the water pressures in the system can be lower than the pressure in the surrounding soil.

1.1   Problems in IWS Systems

IWS has manifold negative effects on residents' health [42]. The periodic filling and draining processes in an IWS system create a humid environment that is conducive for microbial regrowth in pipes, leading to a high rates of morbidity in IWS consumers [13]. Numerous studies assert that IWS systems are strongly related to waterborne
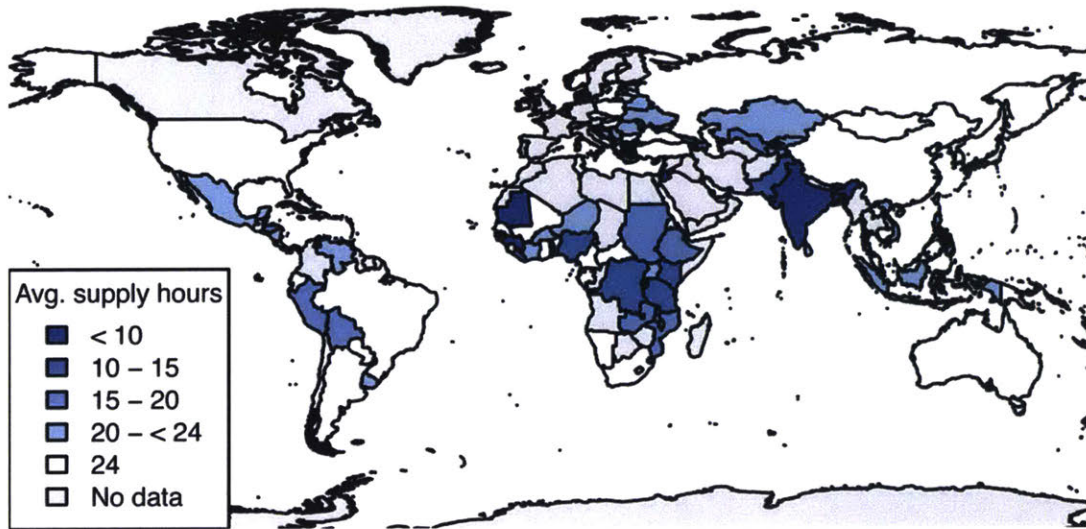
Figure 1-1: IWS situation worldwide in 2015 [54]
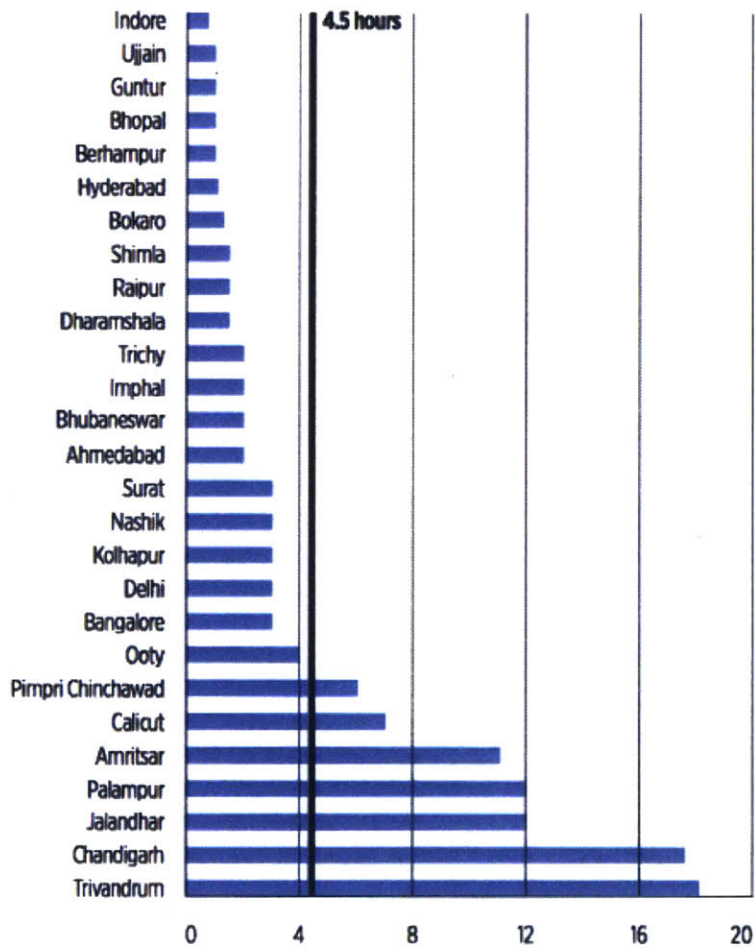
Figure 1-2: IWS in India cities (International Water Association, 2016)

illnesses and diarrheal diseases, including amebiasis, typhoid, cholera and infectious hepatitis [24, 32, 15, 1]. For some diseases, the morbidity can increase by around 40% when compared with the continuous water supply (CWS) systems [61]. Moreover, when there are cracks in the pipe walls or open joints, the inconsistent water pressure in IWS can allow contaminated water in the surrounding soil to flow into the pipes by back siphoning [13]. These external and internal sources of contaminations affect all end uses from drinking to bathing, and other basic needs [13]. While middle-income and high-income consumers are able to buy small-scale water purification equipment, other low-income residents have to tolerate the poor water quality most of the time [74].

The IWS system systems also have lower pressures during supply periods compared with CWS systems [56, 52, 8]. One of the reasons for this is the behavior of customers. Many households never turn off their taps and each household has its own water storage tank on the roof, and some even use suction pumps to collect more water from pipes [53, 9]. Therefore, the water pressures will decrease very quickly as water goes through the pipes. Moreover, air pockets trapped in IWS pipe networks can increase the roughness of the pipe, which leads to higher friction losses in pipes [50, 75]. All these issues prevent those people who live far from the central distribution point from getting enough water everyday. Field studies show that actual periods of water supply time can be as short as 15 minutes per day for some consumers, forcing them to buy, trade, or even steal to get the water they need.

1.2 Conversion to CWS and Key Problems

Serious leakage is one of the key problems that prevent people from converting from intermittent to continuous water supply operations. In fact, leakage level can be as high as 40%-45% in IWS systems [5]. Currently, finding leakages in the field is a time-consuming process and it mainly relies on manual acoustic detection [83].

In order to diagnose and improve the water supply, it is important to have credible models for the hydraulics of IWS systems that can evaluate time varying processes within the pipe network. Complete hydraulic models must be capable of simulating the filling and draining of the pipes and hence, must address the mixed flow conditions where pressurized and free surface conditions can co-exist within the network. This modeling approach can then diagnose how consumer water demand influences the pressure of the system and can lead to better management of IWS systems. Consequently, understanding the pressure behavior of transient flow is essential to solving the problem of leakage, and it represents a first key step in clarifying the state of the current piping network to prioritize areas for repair. Validation of the pipe network hydraulic models can be accomplished by comparison with actual measurements of pressures during the specified water supply periods.

This thesis describes the development of a mixed, transient flow solver for pipe networks. The model is validated using available data from laboratory models and with pressure measurements from networks in the IWS system in Delhi (Taylor, PhD in progress).

The current research can be compared with prior studies for CWS systems, where steady pressures have been simulated and optimized for demand management [44]. Higher frequency pressure transients have also enabled online detection and localization of pipe bursts [12].

1.3 Structure

The thesis is structured as follows:

Chapter 2 reviews previous models that have been developed to model the transient and mixed flow in pipe networks. The chapter discusses key aspects of the numerical

models and highlights some of the mismatches of the currently available software. The current research extends a prototype mixed flow hydraulic solver developed by Lieb using the Preissmann slot model with a finite volume solver [43].

Chapter 3 gives a description of the method and related algorithms that have been developed for the model. The chapter also describes potential instabilities that can occur.

Chapter 4 provides several validation examples, using published data from a simple lab experiment and pressures measured around a T-junction pipe in an IWS system.

Chapter 5 describes the application of the proposed algorithms to a pipe network with selection of boundary conditions for IWS systems.

Chapter 6 provides summaries, conclusions and recommendations.

Chapter 2

Background and Literature Review

2.1 Modeling of Transient Flow

Although the fluid dynamics in a pipe network can be fully described by Navier-Stokes equations [21], it is more convenient and computationally practical to use the 1D Saint-Venant equations for transient flow in circular pipes that correspond to two sets of hyperbolic partial differential equations describing conservation of mass and momentum:

$$\text{For free surface flow: } \frac{\partial h}{\partial t} + v\frac{\partial h}{\partial s} + \frac{c^2}{g}\frac{\partial v}{\partial s} = 0,$$
$$\frac{\partial v}{\partial t} + v\frac{\partial v}{\partial s} + g\frac{\partial h}{\partial s} = g(i - J_f). \tag{2.1}$$

$$\text{For pressurized flow: } \frac{\partial H}{\partial t} + v\frac{\partial H}{\partial s} + \frac{a^2}{g}\frac{\partial v}{\partial s} = 0,$$
$$\frac{\partial v}{\partial t} + v\frac{\partial v}{\partial s} + g\frac{\partial H}{\partial s} = g(i - J_f). \tag{2.2}$$

s and t are the space and the time dimension, respectively; g is the gravitational acceleration; i is the pipe inclination and J_f is a term representing the frictional losses of energy. For situations with free surface flow, h is the pressure head averaged over the depth of fluid in the pipe and c is the gravity wave speed,which can be calculated as:

$$c = \sqrt{\frac{gA_p}{T}}, \tag{2.3}$$

in which A_p is the cross-sectional area of flow and T is the width of the free water surface. In the pressurized flow equations, H corresponds to water pressure head and a is the the acoustic wave speed, the distance travelled per unit time by an acoustic wave as it propagates through the pipe [59]. The expression of a is

$$a = \sqrt{\frac{g/w}{\frac{1}{K} + \frac{1}{8E}(d_0^4 - d_1^4)}}, \tag{2.4}$$

in which w is the unit weight of water, E is the Young's Modulas of the pipe material and some typical values can be seen in Appendix A, d_0 is the pipe outside diameter, d_1 is the pipe inside diameter, and K is the bulk modulus of water. The elasticity of the pipe wall has a significant effect on the wave speed, but air or gas bubbles have more severe effects. If there is no air trapped in the water, $a \approx 1400m/s$. When the volumetric air content is 1%, $a \approx 122m/s - 181m/s$ [46, 82]. Further calculations can be checked in Appendix A.

2.2 Numerical Methods for Hyperbolic Partial Differential Equations

The standard approach to solve hyperbolic partial differential equations (PDEs) computationally is to discretize the continuous differential equations into discrete algebraic difference equations. Currently, there are three main discretization methods: finite difference method, finite element method and finite volume method.

2.2.1 Finite Difference Method

The finite difference method (FDM) uses difference equations to approach differential equations, and its basis is Taylor's expansion [26]:

$$f(x_0 + dx) = f(x_0) + \frac{f'(x_0)}{1!}dx + \frac{f^{(2)}(x_0)}{2!}(dx)^2 + \\ ... + \frac{f^{(n)}(x_0)}{n!}(dx)^n + R_n(x), \tag{2.5}$$

in which $n!$ is the factorial of n and $R_n(x)$ is a reminder term satisfying $\lim_{n\to\infty} R_n(x) = 0$. Selecting $n = 1$, Equation 2.5 can be rearranged as:

$$f'(x_0) = \frac{f(x_0 + dx) - f(x_0) - R_1(x)}{dx} \approx \frac{f(x_0 + dx) - f(x_0)}{dx} \tag{2.6}$$

By discretizing the computational domain into finite grid cells and represent each grid with a point, Equation 2.6 can be used to approximate the differential equations with the difference between points. The concept of FDM is intuitive, and coding it is simple. However, it is difficult to use FDM in complex situations such as complicated geometries [26]. In addition, imposing different boundary conditions for FDM is also a challenge [78].

2.2.2 Finite Element Method

The finite element method (FEM) is a numerical solver usually used in areas such as structural analysis and heat transfer [35]. FEM divides the continuous region into a series of discrete parts termed as finite elements, and algebraic equations are formed in these small elements to approximate the original differential equations. Since these elements are connected by nodes, the algebraic equations for different elements can be assembled into an equation set to be solved [51]. For specific areas, FEM can increase the mesh density in those areas to get more accurate results [35].

By using finite elements, FEM is capable of taking different material properties and various boundary conditions into consideration easily [51]. Moreover, it is able to

model complex geometries with a good mesh generator [51]. However, the mesh generation is a hidden process completed by the computer with certain rules specified by the modeler, and a complex mesh can make FEM computationally expensive [51].

2.2.3 Finite Volume Method

The finite volume method (FVM) is similar to FDM, which divides the computational domain into discrete grid cells. However, instead of using points to represent each grid, FVM treats each grid cell as a control volume and calculates the integrals of differential equations on the control volume to get algebraic equations [76]. FVM is becoming increasingly attractive in computational fluid dynamics since conservation laws are automatically satisfied in each control volume and are thus satisfied on the whole computational domain, which can only be achieved with fine grids in either FDM or FEM [33].

2.2.4 Convergence Criterion

When FDM and FVM are used to solve hyperbolic partial differential equations, the necessary condition for convergence, the Courant-Friedrichs-Lewy (CFL) condition, should be satisfied [38]. Particularly, in 1D case, CFL can be described as:

$$C = \frac{u\Delta t}{\Delta x} \leqslant C_{max},$$ (2.7)

in which Δx and Δt are the interval of space and time discretizations, respectively. u is the velocity and C_{max} is a constant restricting the ratio. For 1D Saint-Venant equations, $u = |v + a|$, in which v is the water flow velocity and a is the wave speed. Equation 2.7 means that to achieve convergence, the distance that the pressurized wave travels in a time period Δt should be less than a certain ratio, C_{max}, of the grid size Δx.

2.3 Techniques for 1D Saint-Venant Equations

Based on the three numerical methods mentioned above, there are a variety of techniques used to solve 1D Saint-Venant equations. The four principle techniques are summarized in the following sections.

2.3.1 Method of Characteristics

The method of characteristics (MOC) is a classical mathematical method to solve 1D Saint-Venant equations[63]. MOC first calculates the characteristic lines and then uses them to degrade Equation 2.1 and 2.2 into a series of ordinary differential equations. If both initial conditions and boundary conditions are given, the equations can be solved along the integral of characteristic lines using a fixed mesh method.
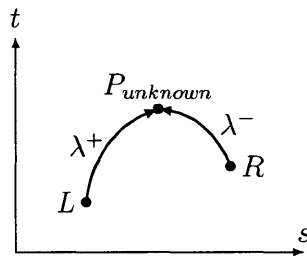
Figure 2-1: The illustration of MOC [62]

Figure 2-1 illustrates necessary elements in the MOC: s and t are the space and time dimension, respectively; L and R are known grid points and P is the grid point to be calculated. Two curves, λ^+ and λ^-, are characteristic lines. For example, the characteristic lines and characteristic equations for free surface flow in a rectangular open channel can be written as:

$$\frac{ds}{dt} = v \pm \sqrt{gh},$$
$$\frac{dv}{dt} \pm \sqrt{\frac{g}{h}}\frac{dh}{dt} = g(i - J_f). \tag{2.8}$$

ds/dt is the gradient of characteristic lines and dv/dt describes how the velocity changes with time. The MOC is a popular method that has been used for over fifty years. It can be found in many textbooks introducing computational fluid mechanics

[47, 62, 71]. However, Cunge (1985) mentions that this method is not applicable to large-scale simulations considering its "numerical instability, programming difficulty and extensive demand of computation capacity" [45]. Generally speaking, the MOC is more suitable for irregular grids due to its flexibility rather than its robustness. Moreover, it is not able to handle situations where free surface and pressurized flows coexist in the same channel.

2.3.2   Shock Capturing Method

The shock capturing method, also known as the interface-tracking method, is an algorithm based on the MOC that is designed to solve transient flow problems [25]. The core idea is to track the movement and locations of the open channel-pressurized flow interface, which separates the fluid into free surface and pressurized flow regimes. The free surface flow is then solved with the MOC and the pressurized flow is solved with the rigid column approach, which ignores the fluid compressibility and pipe wall elasticity. In the rigid column approach, additional pressures caused by water hammer are calculated by Newton's second law as

$$F = ma = \rho A L \frac{dv}{dt},\tag{2.9}$$

in which ρ is the fluid density; A and L is the water column area and length, respectively; dv/dt is the time variation of fluid velocity. For the interface, the model assumes a discontinuity since the gravity wave speed, c, in Equation 2.3 is approaching infinity as the free surface approaches the pipe crown, and a set of mass and momentum equations are established with smaller grids, and specific boundary conditions are also proposed for this zone. This method has some intrinsic limitations such as the requirement for a initial formulation of the open channel-pressurized interface when the pipe is totally empty [79].

Other researchers conducted further research in this field and proposed a "full dynamic" model [55]. instead of filling pipes gradually, this improved model assumes

that the transition from free surface flow to pressurized flow is a fast process creating waves and water hammer effects in a very short time. This phenomenon must be dynamically tracked at each time step. Meanwhile, the complex interaction of shock waves with other elements, such as junctions and reservoirs, is simplified by assigning different boundary conditions. The full dynamic model can address most of the weaknesses that the original shock capturing model has. Nevertheless, it is not widely used since this model assumes that transient flow only exists when water is filling the pipes. This underlying assumption simplifies the problem and decreases the number of equations that must be solved, but it ignores the fact that the transient phase can occur in many situations [79].

2.3.3 Preissmann Slot Model

It can be seen that Equations 2.1 and 2.2 are very similar to each other. Based on this observation, Preissmann [6] suggested combining the two sets of equation by adding a virtual slot to the pipes, as shown in Figure 2-2. Using these assumptions, the free surface flow equation is also applicable to the pressurized flow, whose shock wave speed is represented by the slot width, T_s. The Preissmann slot model (PSM) converts the two-equation transient flow problem into a single-equation set for open channel flow problem, and has been widely adopted by engineers and researchers due to its simplicity. Cunge and Wegner [60] applied PSM in numerical computation with finite difference method and proposed a "Preissmann-Cunger-Wegner" model. Moreover, PSM is used in the Storm Water Management Model (SWMM), software developed by US Environmental Protection Agency (EPA) and widely used worldwide [34, 10, 23, 11].

In contrast to the shock capturing method, the PSM does not need any initial calculations or prior assumptions. Moreover, the single equation set also simplifies numerical solutions. However, it should also be noticed that the PSM has some drawbacks including an inability to simulate negative pressures in pipes and air pockets trapped in pipes.
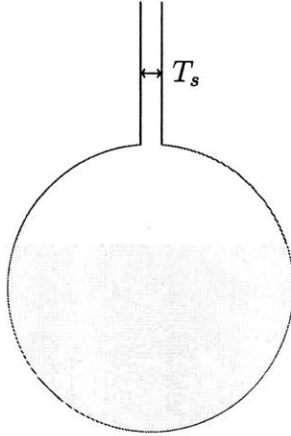
Figure 2-2: Preissmann slot model

The key parameter in the Preissmann slot method is the width of the virtual slot, which is related to the water wave speed, a. It is found that a large wave speed can lead to instabilities, but an artificially low wave speed is not consistent with physics and adds too much virtual water volume in pipes (stored in the slot). In reality, water has an acoustic velocity of approximately 1450m/s, if constrained in pressurized pipes [16]. For the PSM, the wave speed is related to the volume errors in the system. For a certain pressure head and pipe diameter (typically $D \leqslant 1m$), the relationship between wave speed and volume error can be plotted in Figure 2-3, in which H means the pressure head in the pipe. It can be seen that when $a > 100m/s$, the volume error of the pipe system is less than 1%. This provides a reasonable a value.

It should be noted that a small value for a value does not have serious impacts on the simulation for a single pipe, thus many algorithms and simulations can still use a small a to match experimental results [7]. But this choice is not reasonable when simulating a pipe network since the transient pressure is directly proportional to the wave speed. This model is capable of assigning $a = 200m/s$ without harming the stability of numerical results, and it is more realistic considering the air trapped in the intermittent water supply systems.

26
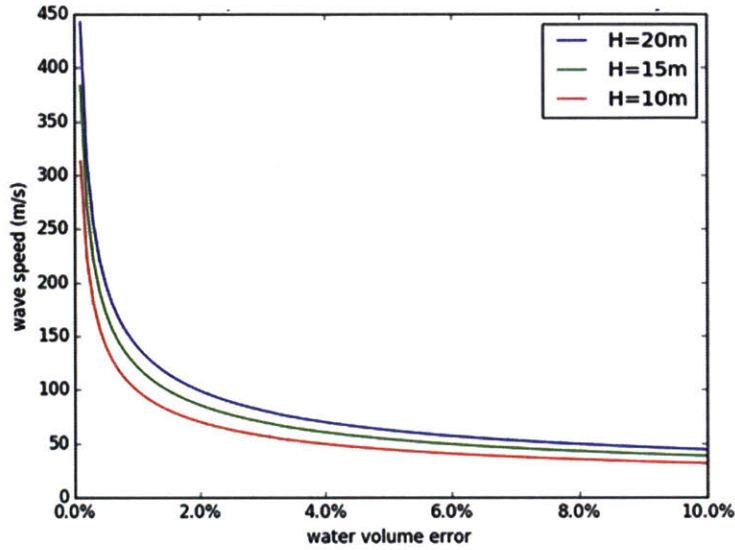
Figure 2-3: Relationship between pipe volume error and wave velocity using Preissmann slot approximation

2.3.4 Two Component Analysis

The Two component analysis (TPA) method was developed to address inabilities of simulating negative pressures within pipes [72, 77]. Although the PSM forces water to be in the narrow slot when pressurized, it is still possible that water drops below the pipe crown but still keeps pressurized if no ventilation is provided. The key difference can be explained in the following equation shared by both the PSM and the TPA method:

$$A - A_t = T_s H_{slot}, \tag{2.10}$$

$$\frac{A - A_t}{A_p} = \frac{g H_{slot}}{a^2}, \tag{2.11}$$

A is the cross-sectional area of water, A_t is the cross-sectional area of the pipe in the PSM, and A_p is the cross-sectional area of the original circular pipe without the slot. Since there is a slot connected at the top of the pipe, A_t is slightly smaller than A_p. T_s is the slot width in the PSM (shown in Fig 2-2), and H_{slot} is the pressure head calculated from the water in the slot. In the PSM, when the pipe is pressurized, $A \geqslant A_p$

is always true, which means that $H_{slot} \geqslant 0$. In the TPA method, H_{slot} is allowed to be less than 0 in order to account for negative pressures. Therefore, when the transition from $A \geqslant A_p$ to $A \leqslant A_p$ happens, the flow regime can either remain pressurized but maintain the negative pressure in the pipe, or change from the pressurized to an open channel flow regime. The latter will occur if there is ventilation along the pipe [77].

The TPA method has become increasingly popular in recent years since it can model negative pressures, but involves an increase in model complexity compared to the PSM. In addition, the TPA method still cannot take air into consideration [72].

2.4   Available Software

This section compares and contrasts some of the existing software programs for modeling hydraulics of pipe networks.

1) EPANET
EPANET is a software package developed by US EPA. It is a pressure driven demand model that can perform extended-period simulations of hydraulic and water-quality behavior within pressurized pipe networks [58]. EPANET has been applied to help design the water supply systems worldwide [57], It uses link-node representation of the whole network. Generally speaking, for each step, EPANET calculates the pressure at each node based on the major and minor loss of energy calculated from the previous time step, and then uses the pressures at nodes to determine the flux in the links [58]. However, EPANET can only be used in the steady state analysis of pressurized pipes.

2) Storm Water Management Model
The Storm Water Management Model (SWMM) was also developed by US EPA. It is usually used to assist the design and analysis of stormwater runoff combined with drainage systems in urban areas [23]. It uses the PSM with a finite difference method

to solve the 1D Saint-Venant equations, and it also uses the link-node representation of the network similar to EPANET. Each time step is divided into two half steps. For the first half step, the flow rates in the links are decided based on the preceding pressures at nodes at first, and the node pressures are then calculated with the average value of the preceding and current half-step flow rates. For the second half step, the flow rates in the links is decided based on the half-step node pressures, and node pressures are then calculated with the average value of the preceding and current full-step flow rates [23]. SWMM is only designed for pipe networks, and there is no spatial discretization within the pipes between nodes. Therefore, it cannot model the dynamics of water waves in single pipes

3) Illinois Transient Model (ITM)

The llinois Transient Model (ITM) was developed by Leon at the University of Illinois [14]. The most updated version solves the 1D Saint-Venant equations with shock capturing method and finite volume method. It is designed for modeling the hydraulic dynamics of water waves in single pipes, but the largest-scale pipe network published from this model has less than 20 pipes, and the computational inefficiency prevents its further application in large-scale networks.

The restrictions of these models prevent them from being used in modeling IWS systems, and their source codes are not readily amendable for further improvements. To address these limitations, Lieb [43] built an open source prototype program that is designed for single pipes and can be scaled to large networks efficiently. To illustrate these models' abilities to solve transient flow problems in different situations, a comparison among these programs are listed in Table 2.1 except EPANET, which can only be used in steady state analysis.

Table 2.1: Comparison among different softwares modeling the transient flow in pipe networks

Software	SWMM	ITM	Lieb's model
Dry pipes	✓	✓	✗
Two-pipe junctions	✓	✓	✓
Three-pipe junctions (mass conservation)	✓	✓	✓
Three-pipe junctions (momentum conservation)	✓	✓	✗
Three-pipe junctions (energy conservation)	✓*	✓*	✗
Looped network	✓	✓	✗
Water hammer effects	✗	✓	✓
Subatmospheric pressure	✗	✓	✗
Air pockets	✗	✗	✗
Numerical Oscillation	✓	✓	✗
Short simulation time	✓	✗	✓
Friendly user interface	✓	✓	✗
Readily amendable	✗	✗	✓

* requires manual calibration

2.5 Summary

Three numerical methods have been widely used for solving hyperbolic PDEs. For pipe networks, the fluid dynamics are represented by 1-D Saint Venant equations that can be solved by one of four methods: The MOC, shock capturing method, PSM and TPA. The MOC is flexible, but it is not able to solve for situations when open channel and pressurized regime coexist in the same pipe. The shock capturing method addresses the coexistence problem, but has intrinsic weaknesses when dealing with dry pipes. The PSM and the TPA method introduce a virtual slot and simplify the solutions to the transient flow equations, and PSM has already been successfully applied in SWMM, the commercial software built by US EPA.

In addition, the comparison among different softwares shows that there are no existing tools available to model the large-scale IWS systems both accurately and efficiently. Since Lieb's prototype program has the potential to model single pipes accurately and

large-scale networks efficiently, and we can have access to and modify the source code, further development based on this model is implemented to improve its applicability and accuracy. These contents are introduced in the following chapters.

Chapter 3

Methodology

This research builds on open source software that was developed by Lieb [43] in her recent PhD thesis. We have conducted a detailed investigation of this software and discovered a number of limitations that affect its applications for pipe networks. This chapter summarizes the proposed solutions and flow algorithms that have been implemented for 1) situations with dry pipes; and 2) modeling three-pipe junctions.

3.1 Conservation Form

The object of study in this model is a network with circular water pipes. Assuming incompressible fluid, the model uses the PSM to convert Equations 2.1 and 2.2 to a single equation set:

$$
\begin{align}
\frac{\partial h}{\partial t} + v\frac{\partial h}{\partial s} + \frac{c^2}{g}\frac{\partial v}{\partial s} &= 0, \tag{3.1a} \\
\frac{\partial v}{\partial t} + v\frac{\partial v}{\partial s} + g\frac{\partial h}{\partial s} &= g(i - J_f), \tag{3.1b} \\
\text{For free surface flow:} c &= \sqrt{\frac{gA_p}{T}}, \tag{3.1c} \\
\text{For pressurized flow:} c &= \sqrt{\frac{gA_p}{T_s}}, \tag{3.1d}
\end{align}
\tag{3.1}
$$

in which T is the width of the free water surface and Ts is the preselected slot width. When the water is in the slot, it means that the pipe is actually pressurized. Since the

finite volume method uses integrals on mesh grids instead of discrete points, Lieb[43] rewrites Equation 3.1 in the following form to assist in subsequent calculations [76]:

$$\boldsymbol{q}_t + (\boldsymbol{F}(\boldsymbol{q}))_s = \boldsymbol{S}, \ s \in (0, L), \ t \in (0, T).$$ (3.2)

L is the total length of a pipe, T is the simulation time and $\boldsymbol{q}, \boldsymbol{F}, \boldsymbol{S}$ are

$$\boldsymbol{q} = \begin{bmatrix} A \\ Q \end{bmatrix}, \ \boldsymbol{F} = \begin{bmatrix} Q \\ \frac{Q^2}{A} + gI(A) \end{bmatrix}, \ \boldsymbol{S} = \begin{bmatrix} 0 \\ S \end{bmatrix}.$$ (3.3)

Q is the flux, A is the cross-sectional area of water and $I(A)$ is given by

$$I(A) = A(h(A) - \bar{y}) = \int_0^{h(A)} (h(A) - z)\, l(z)\, dz.$$ (3.4)

As Figure 3-1 shows, $\bar{y}$ is the centroid height of the water, $h(A)$ is the water depth as well as a function of the cross-sectional area of water, z is the variable of integration representing a certain water depth and $l(z)$ is the pipe width at the depth z.
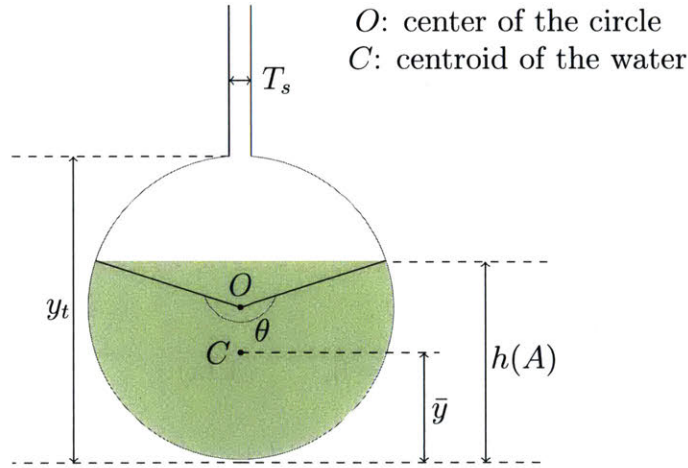
Figure 3-1: Preissmann slot model parameter definition

Since it is difficult to calculate integrals directly in the program, explicit formulas are used to get approximate values. Using A_t to denote the cross-sectional area of the pipe under the slot, there are two situations:

1) If $A < A_t$, the water is below the slot,

$$I(A) = \frac{1}{12} \left[\left(3D^2 - 4Dh(A) + 4h(A)^2 \right) \sqrt{h(A)(D - h(A))} \right.$$
$$\left. - 3D^2 (D - 2h(A)) \arctan \left(\sqrt{\frac{h(A)}{D - h(A)}} \right) \right]. \qquad (3.5)$$

2) If $A \geqslant A_t$, the water is in the slot,

$$I(A) = A_p \left(H_{slot} + \frac{D}{2} \right), \qquad (3.6)$$

where D is the diameter of the pipe. As Equation 2.10 illustrates, A_p is the cross-sectional area of the original circular pipe without the slot, H_{slot} is the pressure head calculated from the water in the slot.

$$A_t = \frac{D^2}{8} (\alpha - \sin(\alpha)),$$
$$\text{in which} \qquad \alpha = 2 \arccos \left(1 - \frac{2y_t}{D} \right), \qquad (3.7)$$

where y_t is the transition height shown in Figure 3-1. Thus the average static pressure, $\bar{p}$, on the whole cross-section can be expressed as

$$\bar{p} = \rho g \frac{I(A)}{A}, \qquad (3.8)$$

where ρ is the fluid density. So the pressure head H is

$$H = \frac{\bar{p}}{\rho g}. \qquad (3.9)$$

The term S (Equation 3.3) includes the friction loss and changes in potential energy:

$$S = (S_0 - S_f) gA, \qquad (3.10)$$

in which S_0 is the pipe inclination and S_f is a term accounting for the friction loss,

the friction loss is empirically calculated by

$$S_f = \frac{M_r^2 Q |Q|}{A^2 R_h \left(A\right)^{4/3}}.$$ (3.11)

M_r is the Manning coefficient which depends on pipe materials, and some typical values are shown in Table 3.1.

Table 3.1: Manning coefficient for some materials [40]

Material	Mr
Brass	0.011
Cast iron, new	0.012
Steel, riveted	0.019
Corrugated metal	0.022
Glass	0.010
Plastic	0.009

R_h is the hydraulic radius and its formula can be written as

$$R_h = \frac{A}{\chi}$$ (3.12)

where χ is the wetted perimeter. For circular pipes, $R_h = D/4$.

3.2 Numerical Schema Using Finite Volume Method

The numerical algorithm in the model with FVM is discussed in the following sections.

3.2.1 Algorithm for a Single Pipe

As shown in Figure 3-2, a single pipe, j, with the length, L_j, can be represented by a line and composing N_j uniform elements with grid length, dx_j. For grid, i, the center coordinate is $(i - \frac{1}{2})dx_j$ and the boundary coordinates are $(i - \frac{1}{2} \pm \frac{1}{2})dx_j$. Lieb uses two ghost cells to represent boundary conditions [43]. They are depicted as dashed lines and numbered with 0 and $N_j + 1$ in Figure 3-2.

36
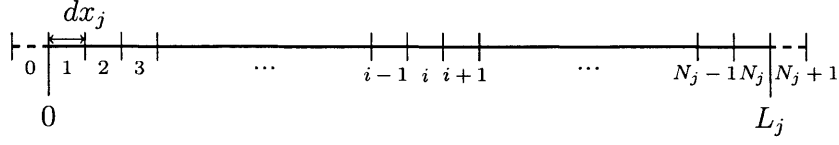
Figure 3-2: Grid discretization of a single pipe j

In this section, since all analyses are illustrated for a single pipe, we drop the subscript j. Our goal is to numerically calculate q_i^n, the cross-sectional area of water and the flux, in Equation 3.2 for each grid i and every time step n. The solution is composed of two steps. In the first step, we ignore the S term temporarily and convert Equation 3.2 into a homogeneous equation:

$$q_t + (F(q))_s = 0, \quad s \in (0, L), \quad t \in (0, T),$$ (3.13)

By integrating Equation 3.13 on the computational cell, i, and the time step, n, the system can be rewritten as:

$$E_c(q_i^n) = q_i^n - \frac{dx}{dt}\left(F_{i+\frac{1}{2}}^n - F_{i-\frac{1}{2}}^n\right),$$

in which

$$q_i^n = \frac{1}{dx}\int_{x_{i-\frac{1}{2}}}^{x_{i+\frac{1}{2}}} q(x,t)dx$$ (3.14)

$$F_{i\pm\frac{1}{2}}^n = \frac{1}{dt}\int_{t_n}^{t_{n+1}} F\left(q\left(x\pm\frac{1}{2}, t\right)\right) dt$$
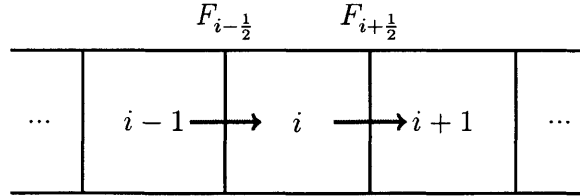
Figure 3-3: Numerical flux F in and out of grid i

As Figure 3-3 shows, $F_{i\pm\frac{1}{2}}^n$ are the time-averaged fluxes at the grid boundaries over a certain time step, and their approximations are termed as numerical fluxes [27]. Lieb [43] chooses Harten-Lax-van Leer(HLL) solver to approximate the actual F value

37

[33]:

$$
\boldsymbol{F}_{i\pm\frac{1}{2}} = \begin{cases} \boldsymbol{F}_L = & \boldsymbol{F}\left(\boldsymbol{q}_L\right) & \text{if} \quad s_L > 0, \\ \boldsymbol{F}_* = & \frac{s_R \boldsymbol{F}_L - s_L \boldsymbol{F}_R + s_R s_L (\boldsymbol{q}_R - \boldsymbol{q}_L)}{s_R - s_L} & \text{if} \quad s_L \leqslant 0 \leqslant s_R, \\ \boldsymbol{F}_R = & \boldsymbol{F}\left(\boldsymbol{q}_R\right) & \text{if} \quad s_R < 0. \end{cases} \tag{3.15}
$$

in Equation 3.15, L and R are abbreviations of left and right, respectively. Hence, $\boldsymbol{q}_R$ and $\boldsymbol{q}_L$ refer to the left and right grids of a certain grid boundary:

$$
(\boldsymbol{q}_L, \boldsymbol{q}_R) = \begin{cases} \left(\boldsymbol{q}_i, \boldsymbol{q}_{i+1}\right) & at \quad i+\frac{1}{2}, \\ \left(\boldsymbol{q}_{i-1}, \boldsymbol{q}_i\right) & at \quad i-\frac{1}{2}. \end{cases} \tag{3.16}
$$

When we have a inclined pipe and inflow from one end, it is possible that some parts are wet while the others are still dry. The dry pipe can cause problems since when $A = 0$ occurs in Equation 3.11, S_f calculation is meaningless (division by zero) and the interface between wet and dry grid can lead to non-existent waves [77]. This problem is not well solved by Lieb, and we adopt the volume-free-surface reconstruction (VFR) method proposed by Begnudelli and Sanders [18, 19] to address it. The core idea is that when the slope exists, there are two different behaviors depending on flow conditions: If water flows steadily in a uniform cross-section, it keeps a constant depth to conserve mass; if water is static, it keeps a constant free surface to conserve energy. A ratio s is used to determine which condition is true at a certain time [19] :

$$
s = \left| \frac{S_f}{S_0} \right| = \frac{M_r^2 Q |Q|}{A^2 R_h \left(A\right)^{4/3} \left| \frac{dz_0}{dx} \right|}, \tag{3.17}
$$

in which z_0 means the invert elevation of the grid boundary and thus $dz_{0,i} = z_{0,i+\frac{1}{2}} - z_{0,i-\frac{1}{2}}$. A certain grid is regarded as wet when its s is larger than a critical value, s^* [77]. After the condition is determined, VFR method reconstructs the water depth at two neighboring grids as:

$$\Delta h_i = \begin{cases} 0, & \text{if} \quad s \geqslant s^* \\ -\frac{\Delta z_{0,i}}{2} \left[1 + \cos \left(\frac{\pi s_i}{s^*} \right) \right], & \text{if} \quad s < s^* \end{cases} \quad \text{(3.18a)}$$

$$h_L^{reconstructed} = h_L + \frac{1}{2} \Delta h_L, \quad \text{(3.18b)} \qquad \text{(3.18)}$$

$$h_R^{reconstructed} = h_R + \frac{1}{2} \Delta h_R. \quad \text{(3.18c)}$$

L and R are abbreviations of left and right, respectively. The reconstructed depth is then used to calculate the cross-sectional area of the water in that grid:

$$A_L = A \left(h_L^{reconstructed} \right) = A \left(h_L + \frac{1}{2} \Delta h_L \right),$$

$$A_R = A \left(h_R^{reconstructed} \right) = A \left(h_R - \frac{1}{2} \Delta h_R \right). \qquad \text{(3.19)}$$

Moreover, for stability issues, we define a minimum restriction, denoted by A_{base}, on A. When A in a certain grid is smaller than this value, we will treat the grid as dry bed. Here we set $A_{base} = 10^{-5}$ and a critical value check is performed:

$$\text{if} \quad A_L < A_{base} \Rightarrow A_L = A(h_L);$$

$$\text{if} \quad A_R < A_{base} \Rightarrow A_R = A(h_R); \qquad \text{(3.20)}$$

$$\text{if} \quad A_L \quad \text{and} \quad A_R < A_{base} \Rightarrow \mathbf{F}_{\frac{L+R}{2}} = \mathbf{0}.$$

Equation 3.20 means that if the reconstructed water depth in a certain grid causes the water cross-sectional area in that grid to be less than the critical value A_{base}, the VFR method should not be used for the grid; if the left and right state of a certain grid boundary are both dry grids, then there is no numerical flux at that boundary. Furthermore, for stability issues, when we find the $E_c(A)$ is less than A_{base}, A is recalculated as

$$E_c^{new}(A_i) = \max \left\{ \frac{E_c \left(A_{\max(1,i-1)} \right) + E_c \left(A_{\min(N,i+1)} \right)}{2}, A_{base} \right\}. \qquad \text{(3.21)}$$

And when Equation 3.21 is triggered, Q is also reevaluated as

$$E_c^{new}(Q_i) = \min \left\{ \frac{E_c\left(Q_{\max(1,i-1)}\right) + E_c\left(Q_{\min(N,i+1)}\right)}{2}, E_c(Q_i) \right\}. \qquad (3.22)$$

For the other parameters in Equation 3.15, s_L and s_R refer to shock speeds. Originally, these two variables can be calculated as

$$\begin{aligned} s_L &= u_L - \Omega_L, \\ s_R &= u_R + \Omega_R, \end{aligned} \qquad (3.23)$$

in which u_i is the flow velocity in grid i, and $u_i = Q_i/A_i$. Ω is calculated as

$$\Omega_i = \begin{cases} \sqrt{\frac{(gI(A_i)-gI(A_*))A_*}{(A_i-A_*)A_i}}, & \text{if} \quad A_* > A_i + \epsilon, & (3.24\text{a}) \\ c\left(A_i\right) & \text{if} \quad A_* \leqslant A_i + \epsilon, & (3.24\text{b}) \end{cases} \qquad (3.24)$$

$$\text{in which} \quad c\left(A_i\right) = \sqrt{\frac{gA_i}{l(A_i)}}.$$

$c(A_i)$ is the gravity wave speed in grid i, and $l(A_i)$ has been previously explained in Equation 3.4 [64]. In Equation 3.24a, a tiny difference between A_* and A_i, e.g. arising from computer precision, can cause the radicand to be negative.

In order to avoid this condition, a tolerance of $\epsilon = 10^{-8}$ is used here [43]. Lieb [43] also states that ϵ has very little effect on the computation. For A_*, a center state variable at the grid boundary used to help calculate Ω in Equation 3.24, Leon proposed a linearization method, depth-positive condition method and two-rarefaction wave approximation method to determine its value [64], and Lieb [43] uses the linearization method in the code. However, according to Malekpour and Karney [20], when these methods are applied, serious numerical oscillations can occur in the PSM when there is a transition from the free surface to pressurized regimes, not only because the numerical solution is not as accurate as analytical solution, but also because the sudden change from gravity wave speed to pressurized pipe acoustic wave speed

cannot be represented in these methods. Therefore, we adopt the method proposed by Malekpour and Karney [20] to replace Lieb's choice [43] for the purpose of suppressing these oscillations. Equation 3.24 is only used when the water is below the slot, and A_* is calculated with an empirical method:

$$A_* = K_a \max \left\{ A_{i-N_S}, A_{i-N_S+1}, ..., A_{i+N_S} \right\}, \tag{3.25}$$

where K_a and N_S are dimensionless empirical values that should satisfy the following restrictions [20]:

$$1.0 \leqslant K_a \leqslant 1.6$$
$$N_S \geqslant 6 \tag{3.26}$$

We run considerable numerical simulations with different K_a and N_S to check the severity of numerical oscillations and calibrate these two parameters as

$$K_a = 1.11, N_S = 6 \tag{3.27}$$

Malekpour and Karney [20] also states that when the water is in the slot, Equation 3.24 is replaced with

$$\Omega_i = a, \tag{3.28}$$

in which a is the wave speed.

After getting q_i^n from Equation 3.13, we can now take the vector S into consideration. According to Equation 3.2 and 3.3, since the first element of the vector S is 0, only the second element of q, the flux Q, is influenced by S. Lieb [43] uses the second-order Runge-Kutta discretization method [41] to update the Q value:

$$E_S\left(Q_i^n\right) = Q_i^n + dt S(q_i^n + \frac{dt}{2} S\left(q_i^n\right)). \tag{3.29}$$

Capart et al. [84] propose that the vector S should also be updated in accordance with the transition between dry and wet conditions, so S_0 is further modified and

adapted for the Preissmann slot:

$$(S_0)_i = -\frac{1}{dx} \left[I \left(h_i + \frac{1}{2}\Delta h_i \right) - I \left(h_i - \frac{1}{2}\Delta h_i \right) \right],$$

$$\text{in which} \quad \Delta h_i = -dz_{0,i}.$$

(3.30)

Similar to Equation 3.20, we check that if either one of $h_i \pm \frac{1}{2}\Delta h_i$ is smaller than the h_{base} corresponding to A_{base}, then the modification of S_0 in Equation 3.30 should be dropped, and $(S_0)_i = -dz_{0,i}/dx_i$ is used instead.

Therefore, by combing 3.14 and 3.29, a complete update formula for q_i^n can be written as

$$E\left(q_i^n\right) = E_s\left(E_c\left(q_i^n\right)\right).$$

(3.31)

Furthermore, the discretization method used to approach continuous differential equations can cause the continuous medium (e.g. fluid) to perform a higher diffusivity, known as the numerical diffusion phenomenon [76]. Hence, Lieb [43] uses an explicit third-order Runge-Kutta total variation diminishing (TVD) scheme [22] to decrease numerical diffusions and capture sharper shock predictions:

$$
\begin{aligned}
q_i^{n+\frac{1}{4}} &= \frac{3}{4}q_i^n + \frac{1}{4}E\left(q_i^n\right), \\
q_i^{n+\frac{1}{2}} &= \frac{1}{3}q_i^n + \frac{2}{3}E\left(q_i^{n+\frac{1}{4}}\right), \\
q_i^{n+1} &= q_i^{n+\frac{1}{2}}.
\end{aligned}
$$

(3.32)

3.2.2 Algorithm for Single Pipe Boundary Conditions

Boundary conditions are crucial to the whole hydraulic model. It can be seen in Figure 3-2 that in this model, boundary conditions are specified using ghost grids at both ends of a pipe, indexed as grid 0 and grid $N + 1$ [43]. According to previous discussions, it is easy to understand that boundary conditions are used to set q values in ghost grids to calculate the numerical flux from the ghost grid, 0, to the first interior grid and from the last interior grid to the ghost grid, N+1. That is, $F_{\frac{1}{2}}$ and

42

$F_{N+\frac{1}{2}}$ are determined by the boundary values.

Whatever the boundary condition is, we always need to have both A, the cross-sectional area of water, and Q, the flux, values in the ghost grid to get the numerical flux F. Generally, the model classifies boundary conditions into four categories [76]. The majority of boundary conditions' specifications and calculations are based on Lieb's analysis[43], and we make some corrections for improvement.

1) Free Flow

Free flow means that all the water can flow out of the pipe without any restrictions. Mathematically, this is expressed by:

$$
\begin{aligned}
Q_{ext} &= Q_{last}, \\
A_{ext} &= A_{last}.
\end{aligned}
\tag{3.33}
$$

The subscript ext refers to the external ghost grid, and subscript $last$ refers to the closest interior grid. This condition represents the situation that water flows out of the open channels.

2) Reflection Flow

Reflection flow condition occurs when water is reflected at the end of the pipe due to a closed valve. The mathematical formula is

$$
\begin{aligned}
Q_{ext} &= -Q_{last}, \\
A_{ext} &= A_{last}.
\end{aligned}
\tag{3.34}
$$

This condition also represents the situation when there are dead end pipe links or when valves are closed within the pipe network.

3) Orifice Flow

Orifice flow occurs when water flows out from a pressurized pipe. There are many formulas to calculate the flux. Lieb [43] uses

$$Q_{ext} = 0.78A(\tau)\sqrt{2g\left(h(A_{last}) - 0.83\tau\right)}, \tag{3.35}$$

where τ is the orifice opening and $\tau \leqslant$ pipe diameter [7]. This boundary condition can simulate conditions of actual demand at the end of a pipe.

4) Specified $Q_{ext}(t)$

When we only have $Q_{ext}(t)$, then $A_{ext}(t)$ should be decided accordingly. To calculate $A_{ext}(t)$, Lieb [43] proposes to check a compatibility equation arising from Riemann invariant [39], a mathematical transformation that can make conservation equations easier to be solved:

$$\frac{Q_{ext}^n}{A_{ext}^n} \pm \phi\left(A_{ext}^n\right) = \frac{Q_{last}^n}{A_{last}^n} \pm \phi\left(A_{last}^n\right),$$
$$\phi(A) = \int \frac{c}{A}dA, \tag{3.36}$$

in which c is the wave velocity, n means a certain time step. If we can recursively find A_{ext}^n that makes the above equality true, then the root A_{ext}^n is what we need for this step. Otherwise, we assume that when a boundary influx is specified, enough pressure is provided to fill the inflow area, so we set A_{ext}^n as

$$A_{ext}^n = \max\left(A_t, A_{last}^n\right). \tag{3.37}$$

This boundary condition applies when the pipe is connected with a water tower or a booster pump.

3.2.3 Algorithm for Junctions

Junctions are crucial for simulating pipe network, and can be classified according to the number of pipes connected together. Junctions in most pipe networks are two or

three-pipe junctions:

1) Two-Pipe Junctions

A two-pipe junction is treated as an ordinary connection unit if there are no valves or elevation differences available. Note that elevation differences occur extensively in sewer networks, but not in water distribution systems. When water flows through this type of junction, it is assumed that the pressure head is unchanged. To provide a mathematical explanation, related variables are introduced in Figure 3-4. Two grids, one is the last grid and the other is the ghost grid of a pipe, are shown for two connected pipes, pipe 0 and pipe 1, respectively. In addition, the boundary numerical fluxes for these two pipes are denoted as $\boldsymbol{F}^0_{boundary}$ and $\boldsymbol{F}^1_{boundary}$.
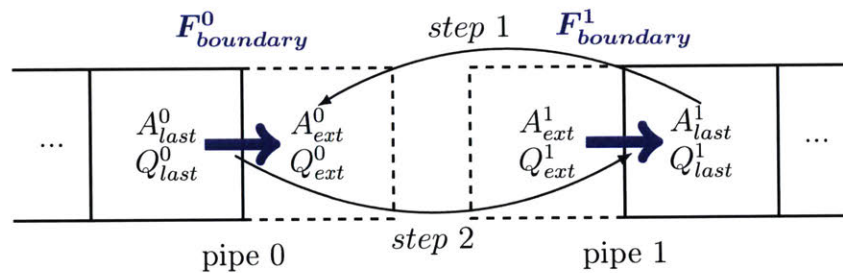
Figure 3-4: Two-pipe junction geometry and related variables

When the model encounters a two-pipe junction with this geometry, it performs a two-step operation. Firstly, it will assume that the water height $h(A^0_{ext}) = h(A^1_{last})$. That is, the model calculates the water height in the last grid of pipe 1 and then assigns this height to the ghost grid of pipe, 0. Also, Lieb [43] set $Q^0_{ext} = Q^1_{last}$ for the mass balance. These are presented as *step* 1 in Figure 3-4. Then $\boldsymbol{F}^0_{boundary}(\boldsymbol{q}^0_{last}, \boldsymbol{q}^0_{ext})$ are calculated, whose value is further assigned to $\boldsymbol{F}^1_{boundary}$. This assignment is called *step* 2. The two arrows show the assignment directions.

2) Three-Pipe Junctions

A three-pipe junction is a complex domain where turbulence happens. Although there are many types of junctions, such as T junctions, Y junctions and so on, T junctions

are most commonly encountered in real pipe networks. Traditionally, local loss coeffi-
cients measured from lab-scale experiments are used to calculate the flow distribution
in junctions. However, this method only applies to steady-state flow distributions.
When it comes to transient flow situation, there is no acknowledged method.

The majority of recent research focused on the gas-liquid two-phase dividing flow
through T junctions[70, 28, 37] and these results, though interesting and impressive,
cannot provide meaningful references for the current research since PSM cannot take
air into consideration. Leon et al. [65] propose a junction algorithm for the drop-shaft
in sewer networks. The algorithm uses mass conservation and y-momentum balance
equations in the junction, but it does not have ghost grids to serve as boundaries and
thus cannot be embedded in Lieb's code. Lieb [43] suggests splitting each connected
pipe into two uniform half pipes from the conduit axis, so the three-pipe junction is
divided into three two-pipe junctions, each one of which is composed of two half pipes.
Then the two-pipe junction algorithm is applied here three times. However, this algo-
rithm fails to conserve energy across the three-pipe junction. Therefore, we propose
to solve the junction problem by setting up basic physical conservation equations.
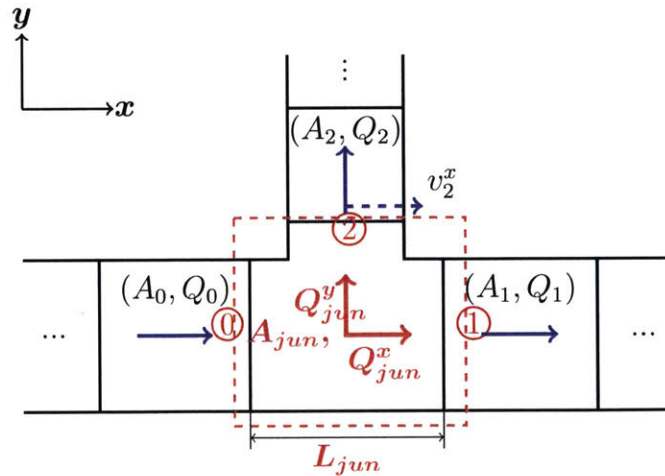

Figure 3-5: T junction geometry and related variables

A basic T junction geometry is shown in Figure 3-5, with three pipe connected. In-
stead of assigning three different ghost cells for each connected pipe, we propose to

define a shared ghost grid (the area within red dashed square) to represent the junction, whose parameters include A_{jun}, L_{jun}, Q_{jun}^x and Q_{jun}^y. Moreover, we set L_{jun} equal to the grid size of pipe 0 .

Three circled numbers refer to different boundaries between the junction grid and pipe grid. If we define positive directions with the coordinate system shown in Figure 3-5, then related variables defined on these boundaries are shown in Table 3.2.

Table 3.2: Variables defined on junction grid boundaries

Boundary	Flux	Flow Area	Normal Vector n	Pressure
⓪	Q_0	A_0	(0, -1)	$p(A_0)$
①	Q_1	A_1	(0, 1)	$p(A_1)$
②	Q_2	A_2	(1, 0)	$p(A_2)$

To get F in and out of this junction, A_{jun}, Q_{jun}^x and Q_{jun}^y need to be solved. These three unknown variable can be solved by equations that consider conservation of mass, momentum and energy. The mass balance equation for transient flow can be expressed as:

$$\frac{\partial(\rho A_{jun} L_{jun})}{\partial t} = \rho Q_0 - \rho(Q_1 + Q_2). \tag{3.38}$$

Momentum balance equation along the x axis for transient flow can be expressed as:

$$\frac{\partial}{\partial t} \int_{CV} v\rho dV + \int_{CS} v\rho v n dA = \sum F_{CV}, \tag{3.39}$$

where CV is the abbreviation of "control volume" and CS is the abbreviation of "control surface".

n is the outward normal vector of control surface, v is the fluid velocity and F_{CV} is the external resultant force applied on the control volume. By taking expressions from Table 3.2, the specific form of Equation 3.39 can be written as

$$\frac{\partial}{\partial t}\left(\rho\frac{Q_{jun}^x}{A_{jun}}A_{jun}L_{jun}\right) = p\left(A_0\right)A_0 - p\left(A_1\right)A_1$$
$$+\rho\frac{Q_0^2}{A_0} - \rho\frac{Q_1^2}{A_1} - \rho Q_2 v_2^x \qquad (3.40)$$

Note that v_2^x refers to the axial velocity in pipe 2, and can be decomposed as:

$$v_2^x = \beta_m v_{jun}^x + \beta_b v_{jun}^y = \beta_m\frac{Q_{jun}^x}{A_{jun}} + \beta_b\frac{Q_{jun}^y}{A_{jun}}. \qquad (3.41)$$

Here β_m and β_b are "pressure regain coefficients" [17]. This term is introduced to represent the momentum exchange between the main pipe and branch pipe, and it was initially proposed by Bajura [17] as $v_2^x = \beta v_0$. We modify the original expression here to make the algorithm independent of the flow type and direction. That is, it is applicable to both dividing flows and combining flows from either side.

The third equation is the energy conservation equation. This is derived from Reynold's Transport Theorem:

$$\frac{d}{dt}\int_{CV}\rho e_t dV + \int_{CS}\rho e_t\left(\boldsymbol{v} - \boldsymbol{v}_c\right)\boldsymbol{n}dA = -\int_{CS}\boldsymbol{q}\boldsymbol{n}dA + \int_{CS}\boldsymbol{\sigma}\boldsymbol{v}dA, \qquad (3.42)$$

$$e_t = e + \frac{1}{2}v^2 + gz_0,$$

$$e = c_v Tm.$$

Here e_t is the total energy per unit volume of fluid, e is the internal energy proportional to the temperature, Tm, $\boldsymbol{v}_c$ is the velocity of the moving control surfaces, $\boldsymbol{q}$ is the heating rate into the control volume through control surfaces and $\boldsymbol{\sigma}$ is the environmental pressure on control surfaces. Generally speaking, Equation 3.42 means that the sum of total energy change in the control volume (first term lefthand side of Equation 3.42) and the total energy flows in and out (second term lefthand side of Equation 3.42) is equal to the sum of the heating from the environment (first term righthand side of Equation 3.42) and the work done by the environment on the fluid (second term righthand side of Equation 3.42). Considering the specific situation we

48

face at the junction grid, each term can be specified in Table 3.3. Note that here we should consider the grid as a three-dimensional one.

Table 3.3: Decomposition of terms in energy equation

	e_t	vn	$v_c n$	qn	σv
$CS : \textcircled{0}$	$\frac{1}{2}\left(\frac{Q_0}{A_0}\right)^2 + g\bar{y}_0$	$-\frac{Q_0}{A_0}$	0	0	$p\left(A_0\right)\frac{Q_0}{A_0}$
$CS : \textcircled{1}$	$\frac{1}{2}\left(\frac{Q_1}{A_1}\right)^2 + g\bar{y}_1$	$\frac{Q_1}{A_1}$	0	0	$-p\left(A_1\right)\frac{Q_1}{A_1}$
$CS : \textcircled{2}$	$\frac{1}{2}\left(\frac{Q_2}{A_2}\right)^2 + g\bar{y}_2$	$\frac{Q_2}{A_2}$	0	0	$-p\left(A_2\right)\frac{Q_2}{A_2}$
CS :water surface(ws)	$\frac{1}{2}v_{jun}^2 + gh\left(A_{jun}\right)$	0	$\frac{dh(A_{jun})}{dt}$	0	0
CS :wetted area (wa)	$e_{t,wa}$	0	0	0	$\sigma_{viscous}v_{jun}$
CV :junction (jun)	$\frac{1}{2}v_{jun}^2 + g\bar{y}_{jun}$	-	-	-	-

1) CS and CV are the abbreviation of control surface and control volume, respectively;

2) $\bar{y}$ is the centroid of fluid, and it can be calculated from Equation 3.4 as $\bar{y}_k = h(A_k) - I(A_k)/A_k$;

3) v_{jun} is the total velocity in the junction grid. When all pipes are the same size, $v_{jun}^2 = \frac{\left(Q_{jun}^x\right)^2 + \left(Q_{jun}^y\right)^2}{A_{jun}}$;

4) For CS :water surface, when the junction grid is pressurized, $v_c n = 0$.

The energy terms on the wetted area are often referred to as local loss, and they are difficult to calculate. All the other terms we list are averaged values over the whole control surface or control volume, thus integrals can be calculated directly. For example,

$$\int_{CV} \rho e_t dV = \rho e_t \int_{CV} dV = \rho e_t V.$$

Therefore, the energy conservation can be simplified as

$$\frac{dE_{jun}}{dt} = \dot{E}_{\textcircled{0}} + \dot{E}_{\textcircled{1}} + \dot{E}_{\textcircled{2}} + \dot{E}_{ws} + \dot{E}_{wa}, \tag{3.43}$$

in which

$$E_{jun} = \rho g A_{jun} L_{jun} \left(\frac{\left(Q_{jun}^x\right)^2 + \left(Q_{jun}^y\right)^2}{2g A_{jun}^2} + \bar{y}_{jun} \right),$$

$$\dot{E}_{\textcircled{0}} = \rho g Q_0 \left(\frac{Q_0^2}{2gA_0^2} + H(A_0) + \bar{y}_0 \right),$$

$$\dot{E}_{\textcircled{1}} = -\rho g Q_1 \left(\frac{Q_1^2}{2gA_1^2} + H(A_1) + \bar{y}_1 \right),$$

$$\dot{E}_{\textcircled{2}} = -\rho g Q_2 \left(\frac{Q_2^2}{2gA_2^2} + H(A_2) + \bar{y}_2 \right),$$

$$\dot{E}_{ws} = \rho g L_{jun} \frac{dA_{jun}}{dt} \left(\frac{v_{jun}^2}{2g} + h\left(A_{jun}\right) \right),$$

$$\dot{E}_{wa} = \text{local loss.}$$

By putting the local loss term in the control volume, we can use the explicit forward method to discretize the three equations:

$$L_{jun} \frac{A_{jun}^n - A_{jun}^{n-1}}{dt} = Q_0^{n-1} - \left(Q_1^{n-1} + Q_2^{n-1} \right) \tag{3.44}$$

$$\rho L_{jun} \frac{Q_{jun}^{x,n} - Q_{jun}^{x,n-1}}{dt} = p\left(A_0^{n-1}\right) A_0^{n-1} - p\left(A_1^{n-1}\right) A_1^{n-1} + \rho \frac{\left(Q_0^{n-1}\right)^2}{A_0^{n-1}}$$
$$- \rho \frac{\left(Q_1^{n-1}\right)^2}{A_1^{n-1}} - \rho Q_2^{n-1} \left(\beta_m \frac{Q_{jun}^{x,n-1}}{A_{jun}^{n-1}} + \beta_b \frac{Q_{jun}^{y,n-1}}{A_{jun}^{n-1}} \right) \tag{3.45}$$

$$\frac{E_{jun}^n - E_{jun}^{n-1}}{dt} = \dot{E}_{\textcircled{0}}^{n-1} + \dot{E}_{\textcircled{1}}^{n-1} + \dot{E}_{\textcircled{2}}^{n-1} + \dot{E}_{ws}^{n-1}, \tag{3.46}$$

in which

$$E_{jun}^n = A_{jun}^n L_{jun} \left[\frac{\left(v_{jun}^n\right)^2}{2g} + \bar{y}_{jun}^n + loss \right],$$

$$E_{jun}^{n-1} = A_{jun}^{n-1} L_{jun} \left[\frac{\left(v_{jun}^{n-1}\right)^2}{2g} + \bar{y}_{jun}^{n-1} \right],$$

$$\dot{E}_{\textcircled{0}}^{n-1} = Q_0^{n-1} \left[\frac{1}{2g} \left(\frac{Q_0^{n-1}}{A_0^{n-1}} \right)^2 + H(A_0^{n-1}) + \bar{y}_0^n \right],$$

$$\dot{E}_{\textcircled{1}}^{n-1} = -Q_1^{n-1} \left[\frac{1}{2g} \left(\frac{Q_1^{n-1}}{A_1^{n-1}} \right)^2 + H(A_1^{n-1}) + \bar{y}_1^n \right],$$

$$\dot{E}^{n-1}_{\textcircled{2}} = -Q_2^{n-1}\left[\frac{1}{2g}\left(\frac{Q_2^{n-1}}{A_2^{n-1}}\right)^2 + H(A_2^{n-1}) + \bar{y}_2^n\right],$$

$$\dot{E}_{ws}^{n-1} = L_{jun}\frac{A_{jun}^n - A_{jun}^{n-1}}{dt}\left[\frac{(v_{jun}^{n-1})^2}{2g} + h\left(A_{jun}^{n-1}\right)\right].$$

Considering that we always use the velocity head to empirically account for the local loss at junctions, the local energy loss is expressed as

$$\text{Loss} = k_m\left(\frac{Q_{jun}^x}{A_{jun}}\right)^2 + k_b\left(\frac{Q_{jun}^y}{A_{jun}}\right)^2, \tag{3.47}$$

in which k_m and k_b are two coefficients that need to be calibrated. For the four parameters, $\beta_m, \beta_b, k_m, k_b$, introduced in Equation 3.41 and 3.47, we use control variate method to study the influences of each individual variable, and then tune them to match the experimental data reported in the literature. For example, for the dividing flow scenario where water flows into pipe 0 and then flows out from pipe 1 and 2, the influences of each variable can be described in Table 3.4. Note that the branch flow ratio is the ratio of the water flows out of the branch pipe to the total inflow.

Table 3.4: Influences of parameters on loss coefficients for the main and branch pipes

Loss coefficient	Branch flow ratio	$\beta_m \uparrow$	$\beta_b \uparrow$	$k_m \uparrow$	$k_b \uparrow$
K_{main}	< 0.5	$\uparrow$	-	-	-
	> 0.5	$\uparrow$	$\uparrow\uparrow$	-	-
K_{branch}	< 0.5	$\downarrow\downarrow$	$\downarrow$	$\uparrow\uparrow$	$\uparrow$
	> 0.5	-	$\downarrow$	-	$\uparrow\uparrow$

- means almost no influence;

$\uparrow$ means increase, $\downarrow$ means decrease;

$\uparrow\uparrow$ large increase, $\downarrow\downarrow$ large decrease.

The tuned parameters are listed in Table 3.5 and the comparison between the experimental data and the simulation results are shown in Figure 3-6. The loss coefficients for the main pipe and branch pipe are defined respect to the largest velocity head in the pipe. That is, for the dividing flow, it is defined on the inflow pipe velocity head;

for the combining flow, it is defined on the outflow pipe velocity head.

Table 3.5: Calibrated parameters for the T junction with equal-sized pipes

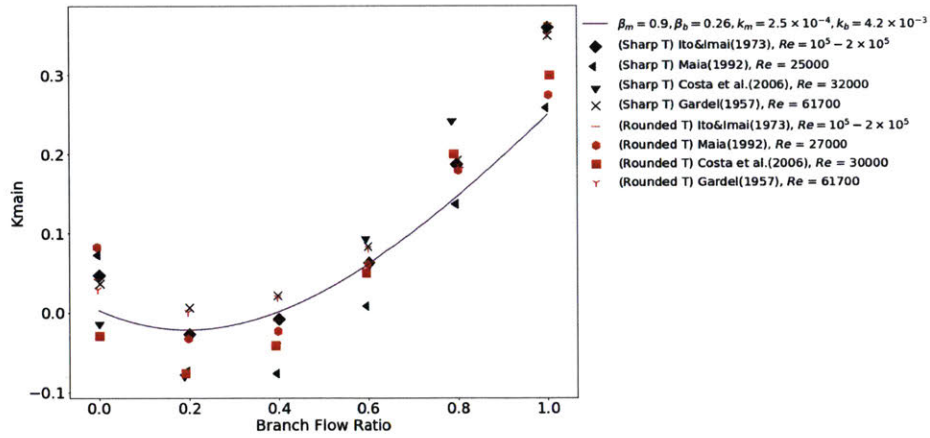| Flow Category	Flow Direction	β_m	β_b	k_m	k_b
Dividing Flow	pipe 0 -> pipe 1, 2	0.9	0.64	2.5×10^{-4}	4.2×10^{-3}
Dividing Flow	pipe 1 -> pipe 0, 2	0.9	0.26	2.5×10^{-4}	4.2×10^{-3}
Combining Flow	pipe 1,2 -> pipe 0	0.5	0.64	2.5×10^{-4}	4.2×10^{-3}
Combining Flow	pipe 0,2 -> pipe 1	0.5	0.64	2.5×10^{-4}	4.2×10^{-3}
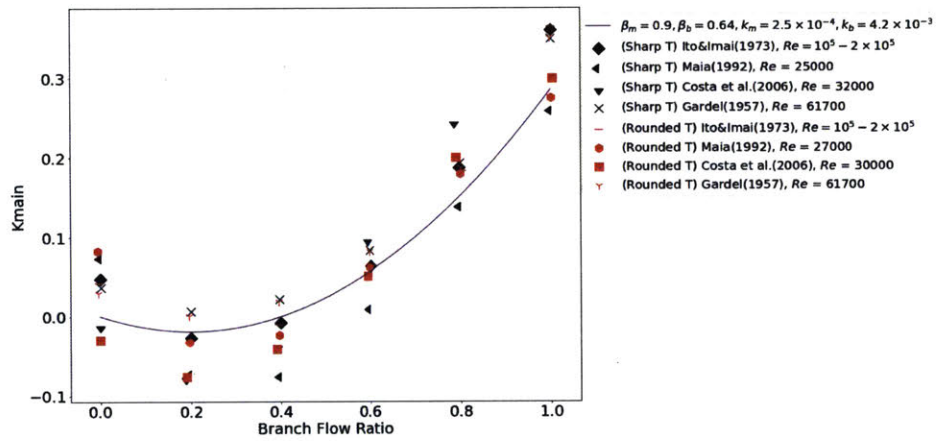
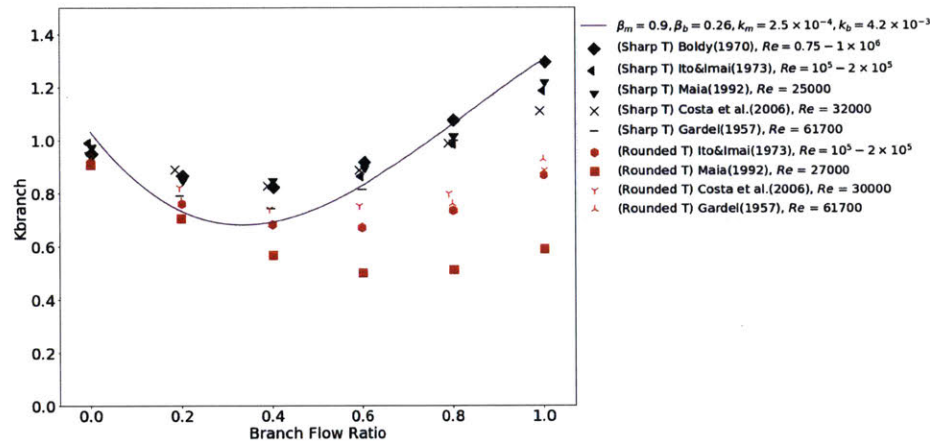1a) Main loss coefficient (pipe 0 -> pipe 1,2)
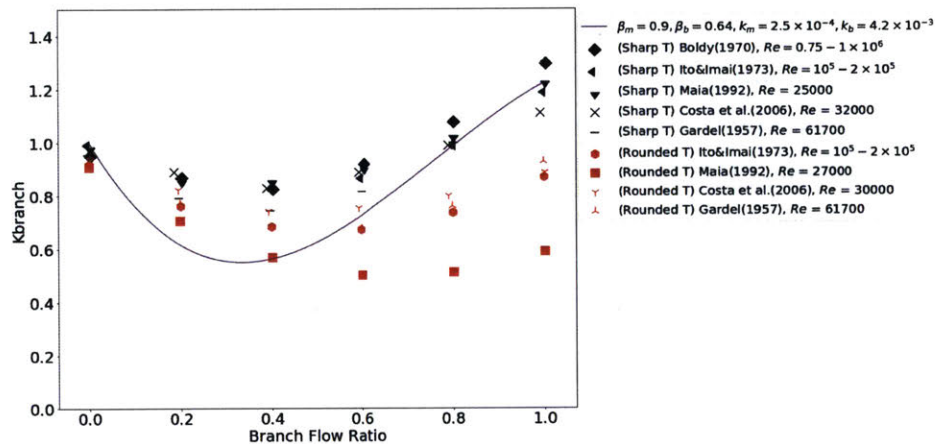
1b) Branch loss coefficient (pipe 0 -> pipe 1,2)

2a) Main loss coefficient (pipe 1 -> pipe 0,2)

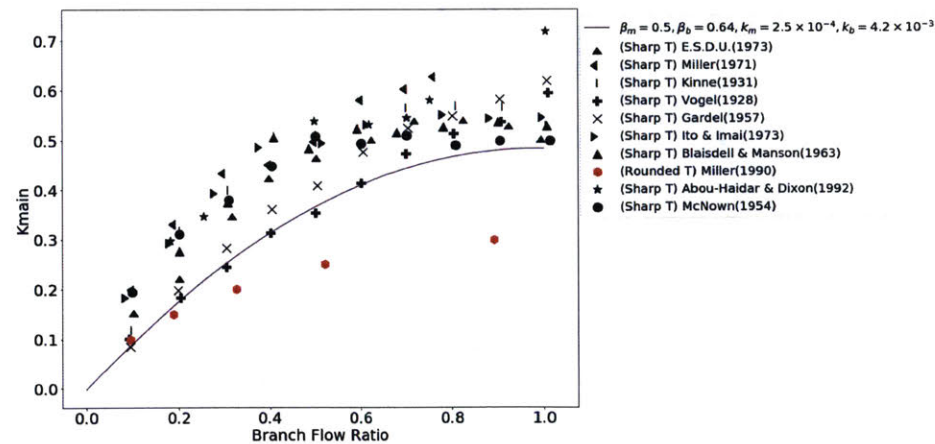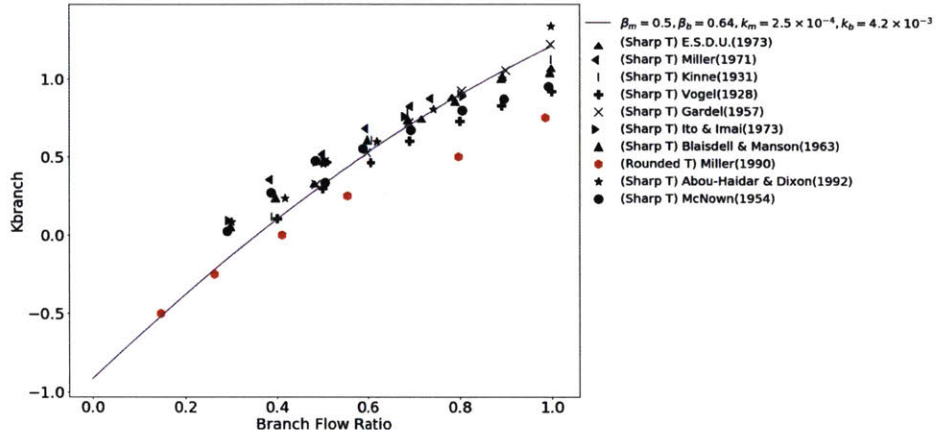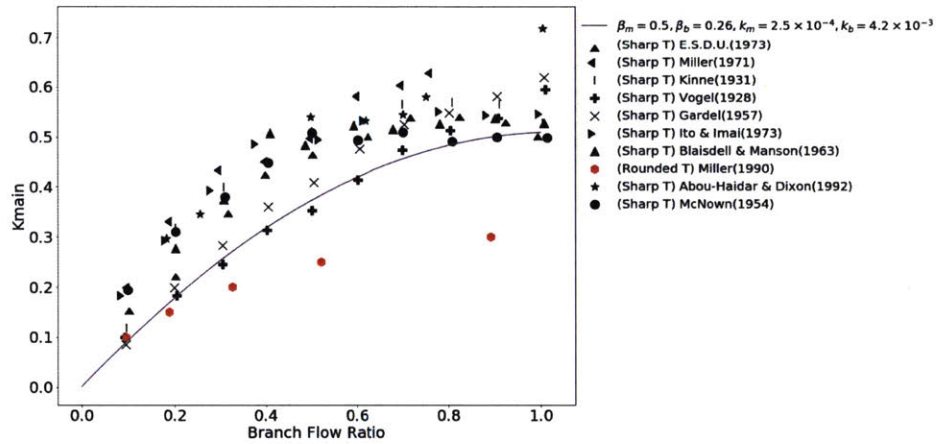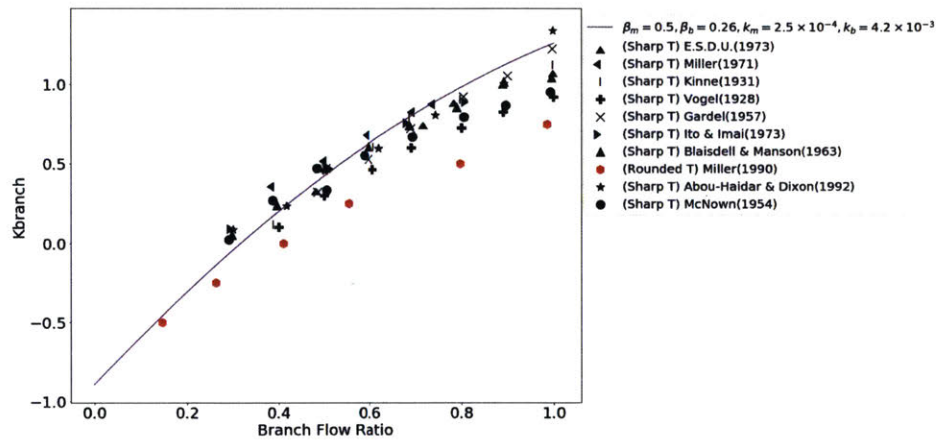2b) Branch loss coefficient (pipe 1 -> pipe 0,2)

3a) Main loss coefficient (pipe 1,2 -> pipe 0)

3b) Branch loss coefficient (pipe 1,2 -> pipe 0)

4a) Main loss coefficient (pipe 0,2 -> pipe 1)

4b) Branch loss coefficient (pipe 0,2 -> pipe 1)

Figure 3-6: Three-pipe junction parameter calibrations, and the experimental data are collected from previous papers [3, 66, 80, 81, 73, 49, 31, 48, 29, 36]

It can be seen that the model achieves a good match with the experimental data for both dividing and combining flows from either side.

Sometimes the branch pipe has a different size from the main pipe. We assume that the center line of main pipe and the center line of the branch pipe share the same elevation, which can be seen from Figure 3-8. If the water depth in the junction is smaller than $(D_0 - D_2)/2$, then the three-pipe junction is the same as a two-pipe junction. Moreover, when the water depth in the junction is larger than the elevation difference, a transitional grid is introduced to incorporate this situation. As Figure 3-7 shows, the grid composed of the black dashed lines has only one variable: A_2^*. Obviously, A_2^* should make the branch pipe 2 has the same water depth as the junction in the main pipe.
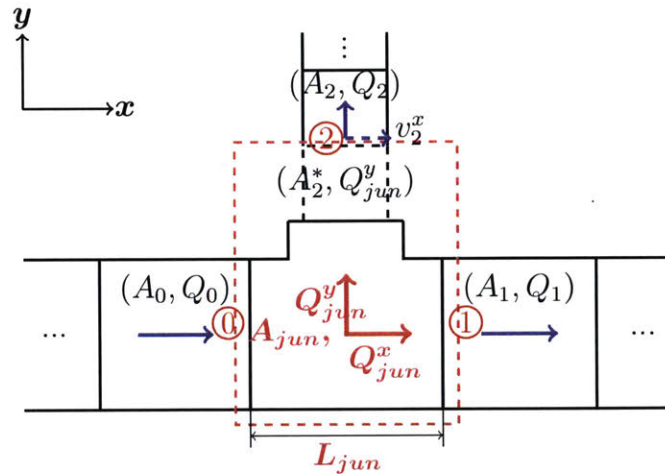

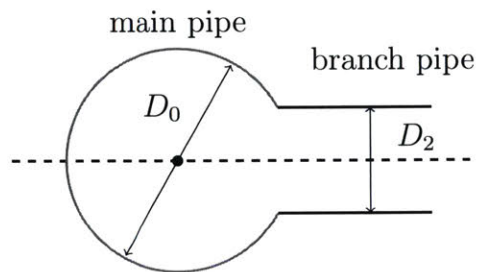Figure 3-7: T junction with a small branch pipe

Figure 3-8: Vertical view of the T junction in Figure 3-7

Again, we hope that the four parameters that we have calibrated for the T junction with three equal-sized pipes can be applied here with reasonable modifications to match the local loss coefficients measured by other researchers. Since the data of the local loss coefficients for the T junction whose branch pipe has a different size from the main pipe is very limited from previous papers, only Gardel's empirical equations of the local loss coefficients and some data from Miller's book are used as the references here [4, 30]. The results of $\beta_m, \beta_b, k_m, k_b$ are presented in Table 3.6.
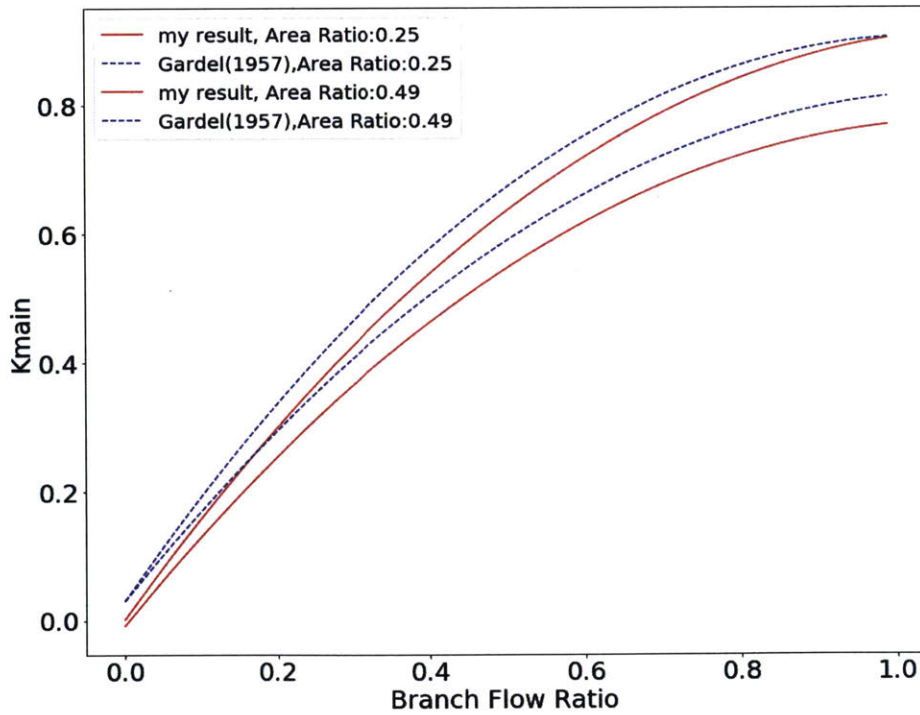
The comparison between the model's results and the results shown by those previous research are presented in Figure 3-9. According to Miller's book in 1990, the loss coefficients of the main pipe in the dividing flow is independent of the branch pipe size [30]. Our model's results are consistent with this statement and the comparison graph is almost the same as Figure 3-6a, so it is not repeated here. In addition, we find that in the dividing flow situation, whether the inflow is from pipe 0 or pipe 1 almost has no influence on the local loss coefficients calculated in this model, and this phenomenon also happens to the combining flow results. Therefore, our plots only distinguish the dividing flow from the combining flow, regardless of their flow directions. Note that the area ratio in Figure 3-9 is calculated as $(D_2/D_0)^2$.

Table 3.6: Calibrated parameters for the T junction with equal-sized pipes

Flow Category	Flow Direction	$beta_m$	$beta_b$	k_m	k_b
Dividing Flow	pipe 0 -> pipe 1, 2	0.9	$0.64\left(\frac{D_2}{D_0}\right)^2$	2.5×10^{-4}	$0.0042\left(\frac{D_2}{D_0}\right)^{1.5}$
Dividing Flow	pipe 1 -> pipe 0, 2	0.9	$0.26\left(\frac{D_2}{D_0}\right)^2$	2.5×10^{-4}	$0.0042\left(\frac{D_2}{D_0}\right)^{1.5}$
Combining Flow	pipe 1,2 -> pipe 0	0.5	$0.64\frac{D_2}{D_0}$	2.5×10^{-4}	$0.0042\frac{D_2}{D_0}$
Combining Flow	pipe 0,2 -> pipe 1	0.5	$0.64\frac{D_2}{D_0}$	2.5×10^{-4}	$0.0042\frac{D_2}{D_0}$
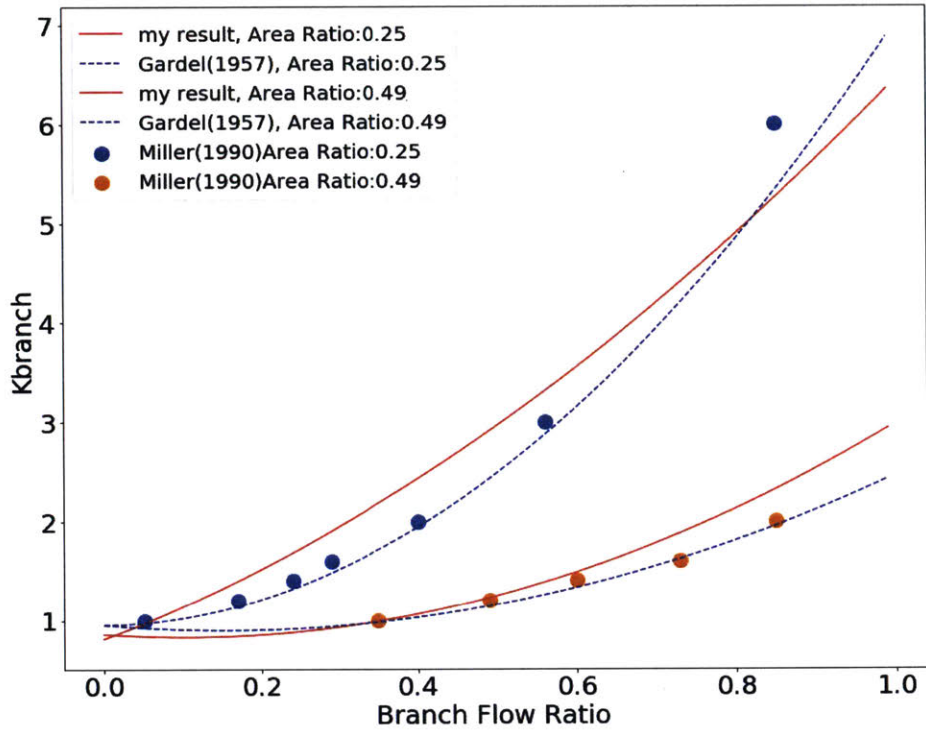
1) Branch loss coefficient (dividing flow)

2a) Main loss coefficient (combining flow)
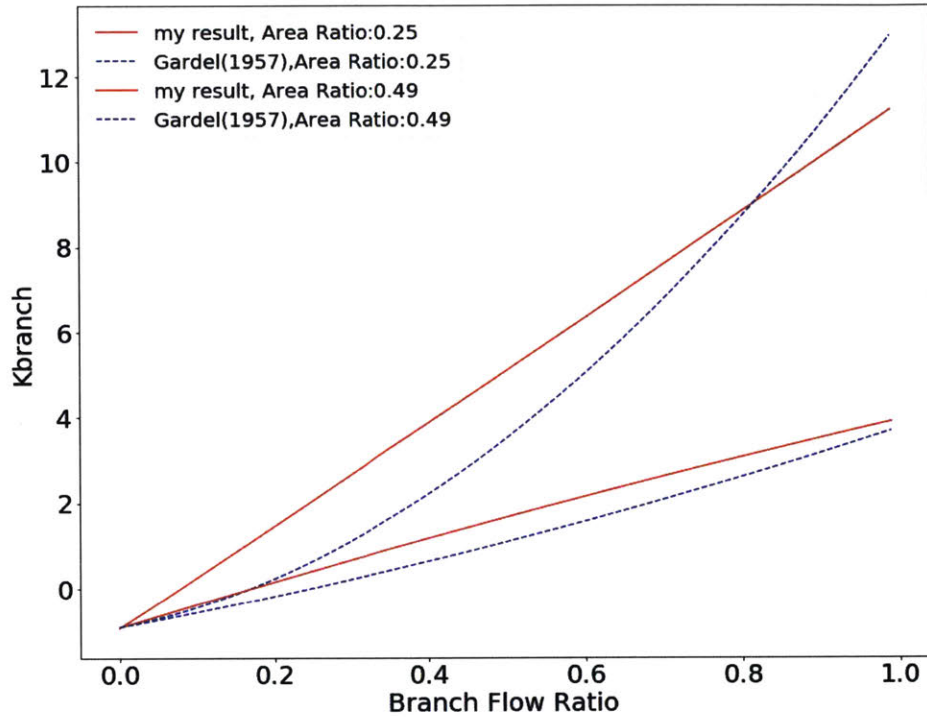
2b) Branch loss coefficient (combining flow)

Figure 3-9: Comparison between the model's results and the previous research for the T junction whose branch pipe has a different size from the main pipe [4, 30]

It can be seen that the model's results are able to match Gardel's and Miller's results to a large extent. Although there are some divergences, it may be explained by the fact that we do not optimize our four parameters to be very complex expressions. In fact, only a simple scaling factor is applied to our results in Table 3.5. Moreover, it is also possible those loss coefficients we used as references from Gardel and Miller are very limited and thus cannot provide a good benchmark. After all, it can be seen in Figure 3-6 that the loss coefficients from experiments do have a certain range of variances. Further analysis shows that for a rusty cast iron (CI) pipe whose length is 200m and whose diameter is 0.3m, the frictional loss coefficient regarding the velocity head is approximately 160. And even if for a new CI pipe with the same length and diameter, the frictional loss coefficient can also be as high as 93. Hence, the divergences here are acceptable.

Moreover, when we are trying to solve unknown junction variables using Equation

58

3.44, 3.45 and 3.46, there are two special cases:

a. If $A_{jun} < 10^{-8}$, it is believed that there is no water in the pipe, then we enforce $A_{jun} = min\{A_0, A_1, A_2\}$;

b. If $\left(Q_{jun}^{y,n}\right)^2 < 0$ happens due to computational accuracy in the process of calculation, we can manually correct it as a tiny value $Q_{jun}^{y,n} = \frac{Q_2}{|Q_2|}10^{-10}$. It also ensures that $Q_{jun}^{y,n}$ has the same sign as Q_2.

After solving $A_{jun}^n, Q_{jun}^{x,n}, Q_{jun}^{y,n}$ from the equation set above, it can be seen from Equation 3.15 that $\boldsymbol{F} = f(\boldsymbol{q}_L, \boldsymbol{q}_R)$, so here $\boldsymbol{F}$ can be expressed as

$$
\begin{aligned}
\boldsymbol{F}_{0|jun} &= f(Q_0, A_0, Q_{jun}^x + Q_{jun}^y, A_{jun}), \\
\boldsymbol{F}_{jun|1} &= f(Q_{jun}^x, A_{jun}, Q_1, A_1), \\
\boldsymbol{F}_{jun|2} &= f(Q_{jun}^y, A_{jun}, Q_2, A_2),
\end{aligned}
\tag{3.48}
$$

where $\boldsymbol{F}_{0|jun}, \boldsymbol{F}_{jun|1}, \boldsymbol{F}_{jun|2}$ refer to the numerical flux from the last grid of pipe 0 to the junction, the numerical flux from the junction to the first grid of pipe 1 and the numerical flux from the junction to the first grid of pipe 2, respectively. If the branch pipe has a different size from the main pipe, we should modify the expression of $\boldsymbol{F}_{jun|2}$ to be

$$
\boldsymbol{F}_{jun|2} = f(Q_{jun}^y, A_2^*, Q_2, A_2).
\tag{3.49}
$$

Furthermore, since a temporary state with three variables $A_{jun}, Q_{jun}^x, Q_{jun}^y$ is introduced in the three-pipe junction algorithm, another communication mechanism is developed to enable the pressure wave to travel through the junctions. That is, this mechanism is utilized to incorporate the coupling effects between the junction and pipes. Since the pressure wave have influences on the cross-sectional area of the water, the algorithm uses this signal to trigger the communication mechanism.

Taking the branch pipe as an example, If $A_2 > (1 + tol)A_{jun}$ for the T junction with equal-sized pipes or $A_2 > (1 + tol)A_2^*$ for the T junction with small branch pipes is found during calculations, the inflow area to pipe 2 is set as A_2 and the influx

is set as a very tiny number. *tol* is a parameter to describe the allowed tolerance error. Simulation results show that a too large *tol* can make the mechanism lose the ability of communication, while a too small *tol* can introduce unnecessary oscillations and instabilities. Therefore, it is empirically set as 5% based on many numerical simulations. Accordingly, the numerical flux for the branch pipe is calculated as

$$\boldsymbol{F}_{jun|2} = f(\frac{Q_2}{|Q_2|}1^{-10}, A_2, Q_2, A_2). \tag{3.50}$$

The same communication mechanism also applies to the other two pipes.

3.2.4   Overview of the Algorithm Procedure

Section 3.2.3 describes the specific algorithms introduced in the model. The whole numerical process can be performed in two steps: 1) calculate boundary numerical fluxes for single pipe junctions (boundary conditions), two-pipe junctions and three-pipe junctions. 2) For interior grid cells, update their values sequentially with Equation 3.32 according to their grid and pipe number. Figure 3-10 shows the two-step process.

3.3   Model Implementation Requirement

The source code is written in C++, and it is embedded in Python with Cython [43]. The input file can be originally exported from the EPANET (.inp file), and this file is then preprocessed to simplify the settings.

When specifying the input parameters for hydraulic models, we should keep in mind that the pipe has its own direction, which is specified by the junction indices at each end. In addition, when building T junctions, it is required in the code that the pipe indices of three connected pipes should be ordered as: inlet pipe > main run > branch pipe. The incorrect indices setup can result in wrong results.
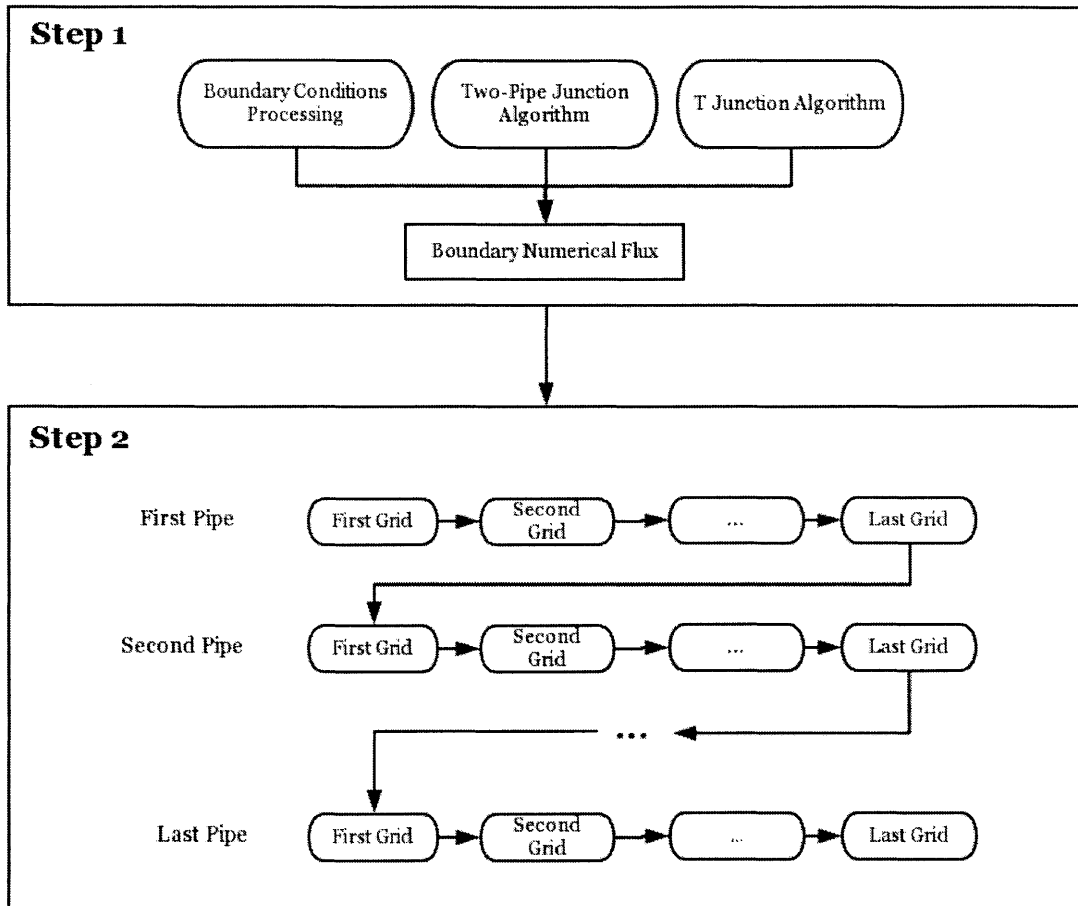
Figure 3-10: Process of the whole model [43]

3.4 Summary

This chapter describes the detailed algorithms used in the proposed transient flow model. It presents the general framework by Lieb [43] at first, and then shows the treatment of dry pipes and the techniques used to suppress numerical oscillations that we adopt for improvement [20]. Moreover, the different boundary conditions are classified into four scenarios and incorporated into the algorithm by Lieb [43]. Further, the algorithms of two-pipe junctions from Lieb [43] and T junctions developed by the author, are shown. In addition, we calibrate the T junction algorithm to match the local loss coefficients from previous experiments. Finally, some modeling tips from

our hands-on experiences are mentioned to help understand the complete modeling procedures.

Chapter 4

Examples of Small-Scale Networks

In this chapter, several examples of small-scale networks are provided to illustrate the model's applicability and accuracy.

4.1 Dry Pipe Experiment Reproduction

The experiment was conducted by Aureli et al. in 2015, and the detailed description can be found in their paper[68]. Generally, the laboratory setup is shown in Figure 4-1.
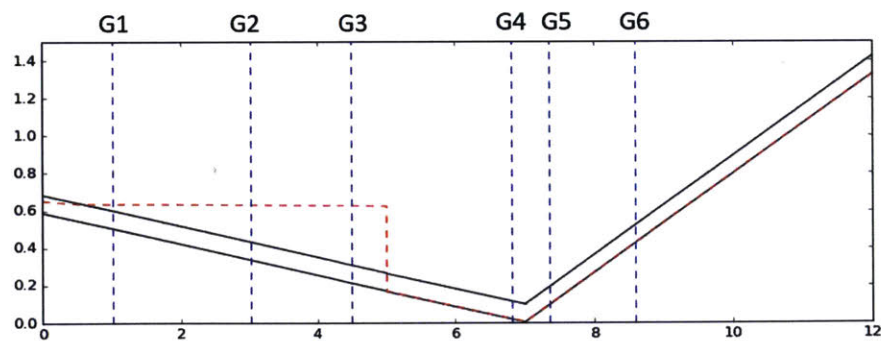

Figure 4-1: Experiment Setup and Initial Conditions of Aureli et al. (2015)

Two solid black lines refer to the pipe invert and crown, the red dashed line is the initial condition of water depth in pipes, and the six blue dashed lines are locations of pressure gauges G1 to G6. All axial numbers are in SI units. The whole pipe

has a length of 12.12m. The first part of the pipe's length is around 7m and slopes downwards at 8.4%. The second part of has a length 5m and slopes upwards at -27.7%. The inner diameter is 0.192m and the wall thickness is 4mm. A valve is placed approximately 5m away before the upstream end and is suddenly opened to allow the water to flow. The location of pressure gauges can be seen in Table 4.1.

Table 4.1: Location of the measuring gauges, x is the distance along pipe axis [68]

Pressure Gauge	x(m)
$G1$	1.00
$G2$	3.00
$G3$	4.50
$G4$	6.80
$G5$	7.32
$G6$	8.52

The left end of the pipe is partly closed to maintain the initial water height in the beginning, and the right end is completely open. Therefore, this experiment is a ventilated system, eliminating possible influences of air pockets.

This experiment mainly aims to study simple transient flow behavior in a single sloped plexiglas pipe. As can be seen, the setup carefully avoids the potential effects from boundary conditions, and the water will oscillate in the pipe after the experiment starts. The six gauges, perpendicular to the pipe axis, are installed at the bottom of the pipe to measure the pressure, equal to the water depth, in 30 seconds. Our numerical model is applied here to reproduce the experimental results. We use $dx = 0.04m, dt = 1/1200s$, and Manning roughness is set to be $Mn = 0.009$ corresponding to plexiglas materials according to engineering charts. Moreover, wave celerity is chosen as $a = 12m/s$ based the authors' description in their paper. The comparison among this model's results, the experimental data and the Aureli et al.'s model results are shown in Figure 4-2. The horizontal line in each graph is the pipe

crown. As can be seen, most of the time our modeling results can match the gauge measurements pretty well. Moreover, Figure 4-2a shows that our model can simulate the sudden pressure drop in the beginning better than the authors' TPA method model. However, Figure 4-2d and Figure 4-2e also show that sometimes our model's pressures are a little higher than the experimental data. This may be because we have the minimum amount of water required in the pipe.

(a) G1 data comparison

(b) G2 data comparison

(c) G3 data comparison

(d) G4 data comparison
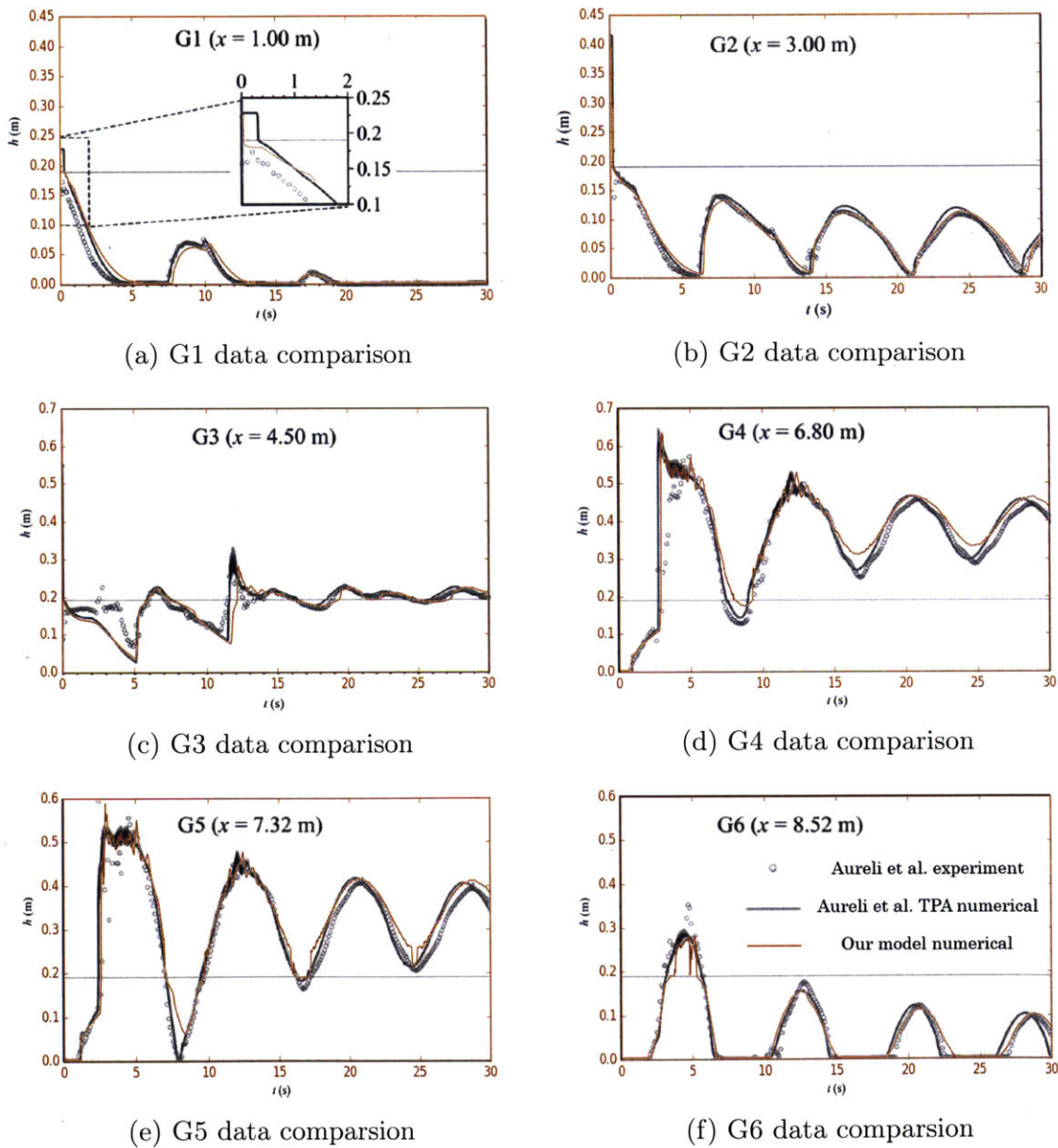

(e) G5 data comparsion

(f) G6 data comparsion

Figure 4-2: Comparison among experimental results [68], Aureli et al.'s TPA simulation and our model's simulation results. Legend is shown in the final subplot.

4.2   Simulations of A Single T Junction

Modeling a pipe network with T junctions is a major concern. As stated in previous chapters, the modeling of T junctions is a tricky problem that has not been well solved in the formulation presented by Lieb [43], and the algorithm described in Chapter 3 for this situation is one of key contributions that this thesis provides. Here a single T junction with different initial conditions and boundary conditions are described to demonstrate the model's ability.

4.2.1   A Single T Junction with Equal-Sized Pipes

A single T junction is shown in Figure 4-3. It has four nodes whose indices range from 0 to 3 and three pipes whose indices range from 0 to 2. For each pipe, the length is 1.5m and the diameter is 0.3m. All the nodes have the same elevations. Figure 4-3 shows a dividing flow situation and the arrows represent the flow directions: node 0 is the inflow node with an inflow velocity of 2m/s, and node 2 and 3 are two nodes set as orifices to allow for the outflow. The wave velocity is 200m/s and the Manning's roughness coefficients are set to be 0.008 for all pipes. The initial condition is set as full pipes with a tiny flow speed. The three blue crosses are the grids where we record the pressure in the model, and the three orange crosses are the grids where we record the flux.
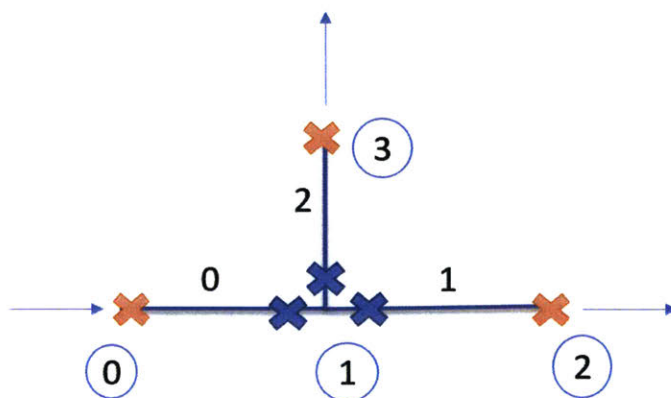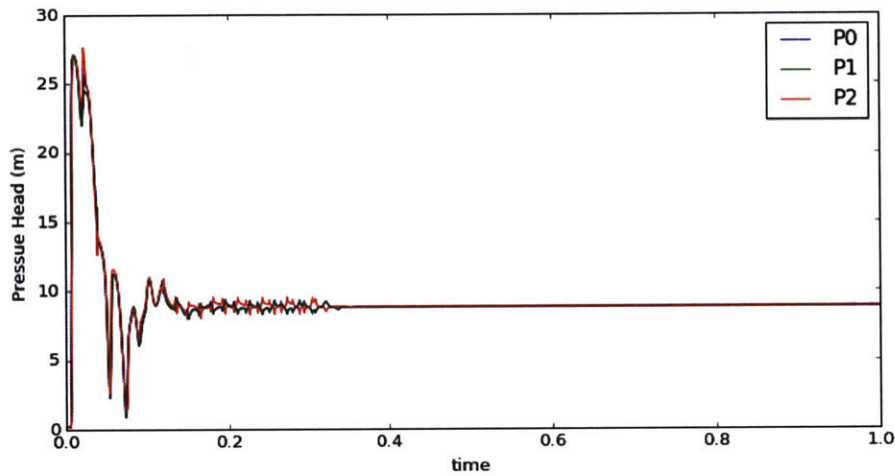

Figure 4-3: T junction

First we close the orifice node 3 and set the opening of orifice node 2 to be 0.1m.

The total simulation time is 1 second. Each pipe is divided into 50 grids and the total simulation time is divided into 20000 steps to satisfy the CFL condition. The corresponding pressures at the blue crosses and fluxes at the orange crosses are shown in Figure 4-4. It can be seen that the sudden inflow pushes the initial water in the pipes to move, creating a high pressure during the transient phase in the beginning before reaching the steady state. Although there is no flow in the branch pipe 2, it sill maintains the same pressure as the other two pipes.

(a) Pressures around the junction

(b) Fluxes in and out of the junction

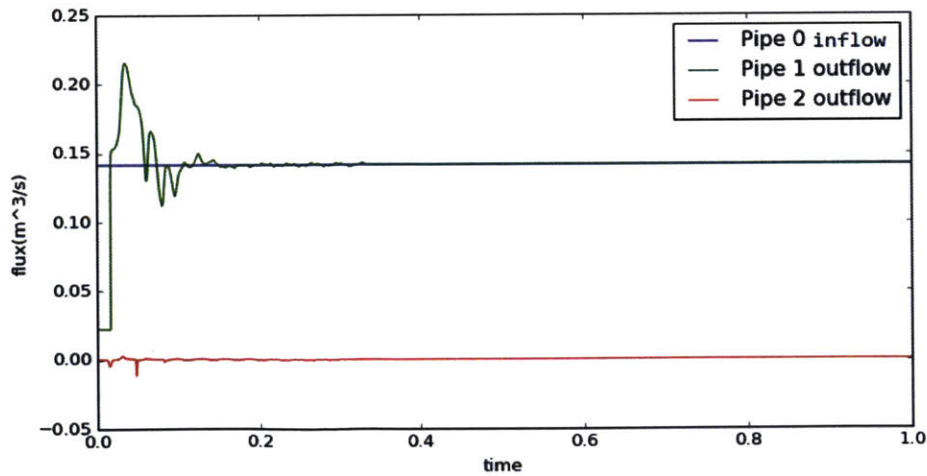Figure 4-4: Pressures and fluxes for a T junction when the branch flow ratio is 0

Second we close the orifice node 2 and set the opening of orifice node 3 to be 0.1m.

The total simulation time is 2 seconds. Each pipe is divided into 50 grids and the total simulation time is divided into 40000 steps to satisfy the CFL condition. The corresponding pressures at the blue crosses and fluxes at the orange crosses are shown in Figure 4-5. With a branch flow ratio of 1, the sudden inflow also creates a high pressure during the transient phase in the beginning, but the pressure pattern is different from the situation that the branch flow ratio is 0. Again, all the three pipes maintain the same pressure near the junction, which is consistent with our intuition.

(a) Pressures around the junction
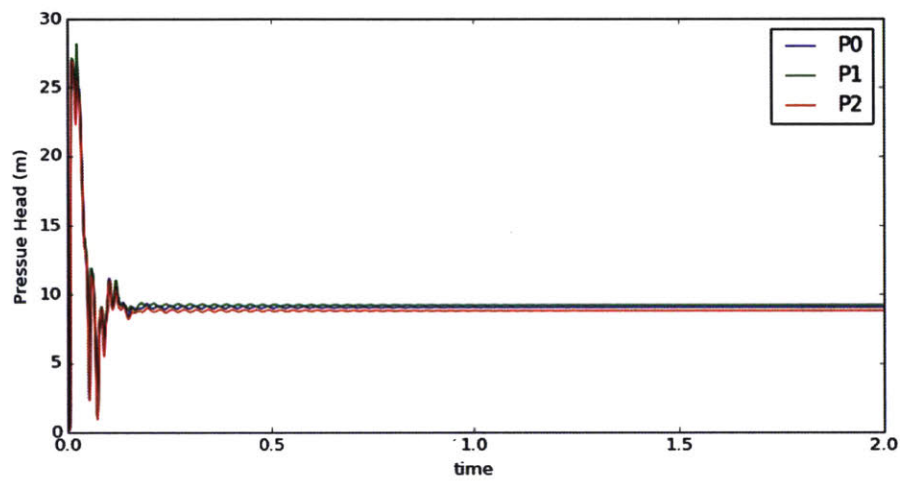

(b) Fluxes in and out of the junction

Figure 4-5: Pressures and fluxes for a T junction when the branch flow ratio is 1
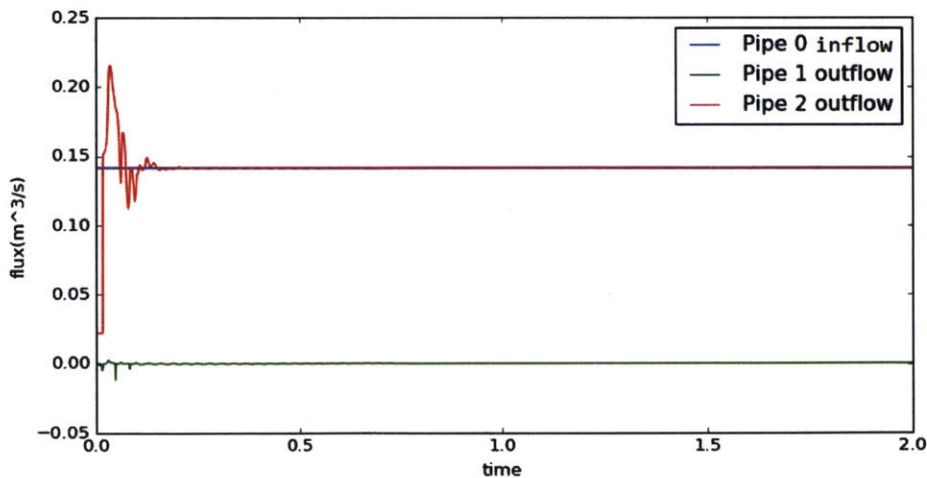
4.2.2 A Single T Junction with Pipes of Different Sizes

The T junction geometry and the flow directions are the same as what is shown in Figure 4-3. For each pipe, the pipe length is 1.5m. For pipe 0 and 1, the pipe diameter is 0.3m, while pipe 2's diameter is 0.15m. The inflow velocity is 3m/s from node 0. The wave speed is 200m/s and the Manning's roughness coefficients are set to be 0.008 for all pipes. The node 2 is set as an orifice with an opening of 0.1m, and the node 3 is set as an orifice with an opening of 0.05m. The initial condition is set as almost dry pipes ($A = 10^{-5}m^2, Q = 10^{-7}m^3/s$).
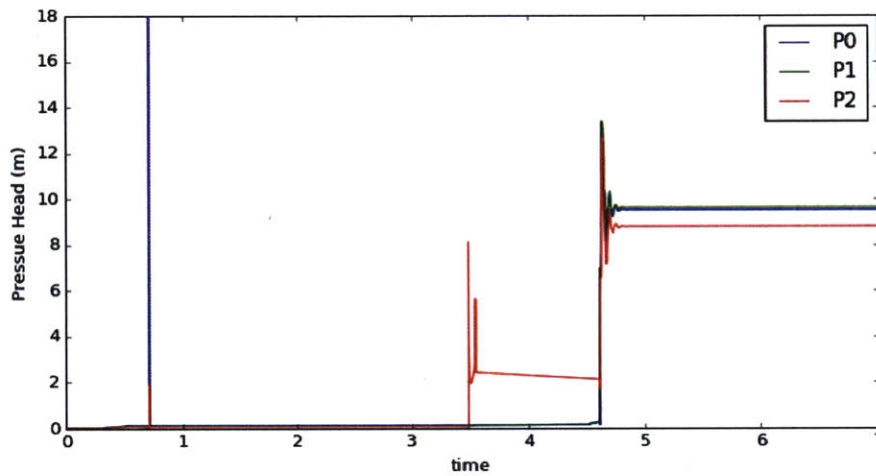
(a) Pressures around the junction

(b) Fluxes in and out of the junction
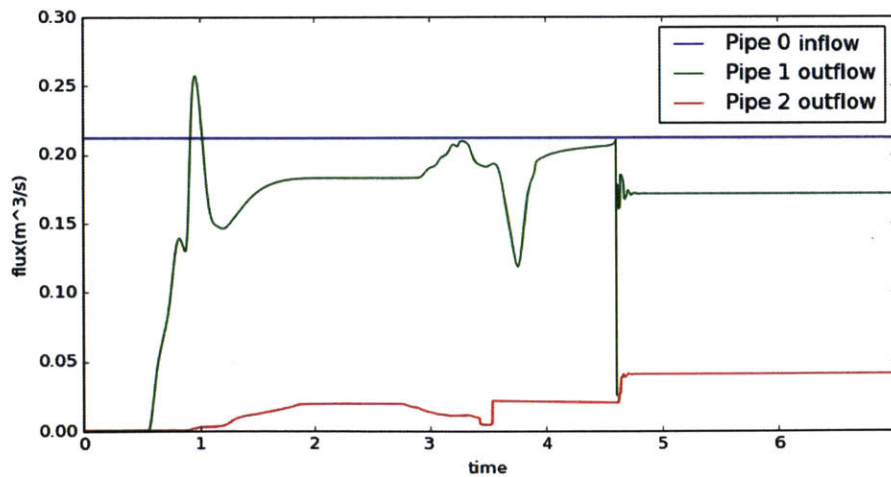
Figure 4-6: Pressures and fluxes for a T junction with different pipe sizes

The total simulation time is 7 seconds. Each pipe is divided into 50 grids and the total simulation time is divided into 140000 steps to satisfy the CFL condition 2.7. Figure 4-6 shows the pressures and fluxes at blue and orange crosses, respectively. It can be seen that the system takes some time to build the pressure. Pipe 2 becomes pressurized at first and then pipe 1 is pressurized. It is also noticeable that there is an unusually high pressure in Figure 4-6a. A closer observation shows that this phenomenon arises from the communication mechanism. As explained in last chapter, the communication mechanism holds the inflow area for the branch pipe until a certain amount of water in the branch pipe is trapped near the junction. The triggering of the mechanism causes oscillations of the pipe pressures in a very short time. It should be taken into considerations in the future if we observe such unusual pressures in the transient state when we are modeling the pipe network in the field. No specific treatment has been designed for it, and removing these data automatically by data comparison would be a useful improvement.

4.3   H-shaped Network

A H-shaped network is built with the model, and the geometry of the network is shown in Figure 4-7. It is composed of six nodes whose indices range from 0 to 5 and five pipes who indices range from 0 to 4. For each pipe, the diameter is 0.3m and the length is 100m except for pipe 4, whose length is 50m. All the nodes have the same elevations. The arrows represent the flow directions: node 0 and 3 are two inflow nodes with an inflow velocity of 2m/s for each node, and node 2 and 5 are two orifice nodes whose openings are both 0.08m. The wave velocity is 200m/s and the Manning's roughness coefficients are set to be 0.008 for all pipes. The initial condition is set as almost dry pipes ($A = 10^{-5}m^2, Q = 10^{-7}m^3/s$). The four blue crosses are the grids where we record the pressure in the model, and the four orange crosses are the grids where we record the flux. Since the pipe network is symmetric, only part of the results are shown here.
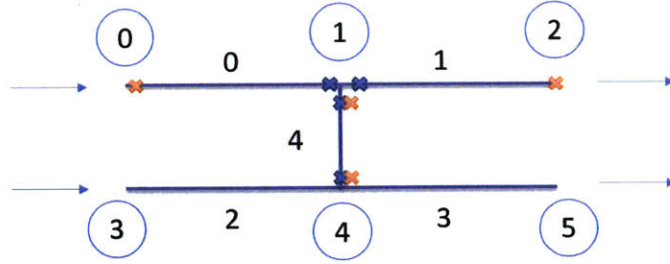
Figure 4-7: H-shaped network

The total simulation time is 400 seconds. The grid size of each pipe is set as 1m and the total simulation time is divided into 100000 steps to satisfy the CFL condition. Figure 4-8 shows the pressures and fluxes at the blue and orange crosses, respectively. Since two grids, one at the beginning of the pipe 4 and one at the end, are recorded and pipe 4's direction is from the node 1 to node 4 based on the descriptions in Chapter 3 of this thesis, the grid close to node 1 is called the "inflow" grid and the grid close to node 4 is called the "outflow" grid. In this situation, the water from pipe 0 is firstly divided into pipe 1 and 4 at the node 1. Meanwhile, the water from pipe 2 is also divided into pipe 3 and 4 at the node 4. In pipe 4, the water comes from the node 1 and node 4 has different flow directions, and the two flows collide with each other in the middle of the pipe 4 and are then reflected back to the junctions. As Figure 4-8c shows, there are some inflow from both ends of pipe 4 between 40 and 80 seconds, and these fluxes disappear due to the collision and later reflections.
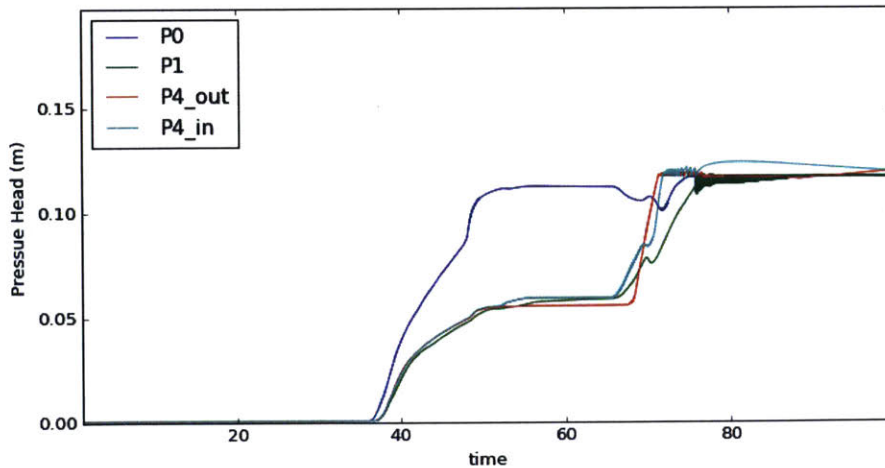
(a) Pressures at the orange crosses for the first 100 seconds

71
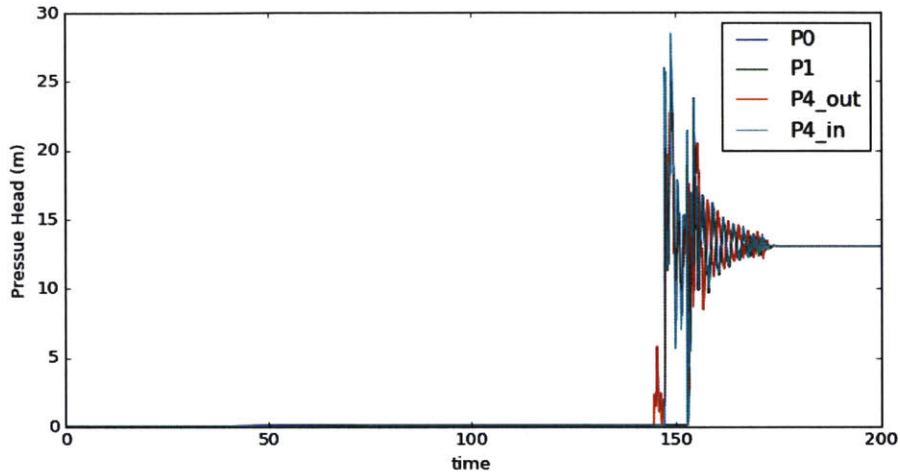
(b) Pressures at the orange crosses for 400 seconds
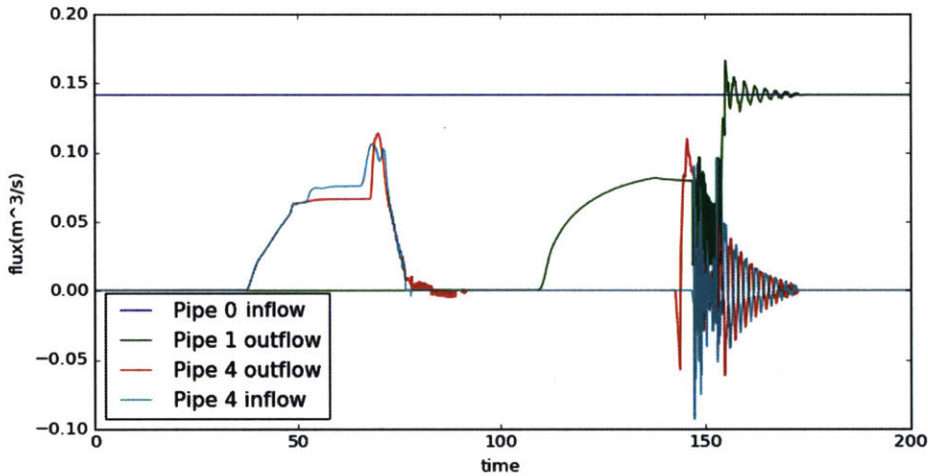
(c) Fluxes at the blue crosses for 400 seconds

Figure 4-8: Pressures and fluxes for a H-shaped network

4.4 Field T Junctions

A field study is conducted at a discrete metered area (DMA), a hydraulically isolated sub-zone in a distribution network, in Delhi. Figure 4-9 shows this situation comprising a main run with many branch pipes connected to deliver water to local households, and a flow meter is available at the beginning of the pipe to monitor the inflow. The supply time for this area is 3 hours/day on average. To keep track of the pressure change in the field, five pressure loggers purchased from Telog are installed

along the trunk main. These loggers can operate in two modes: normal mode (measurements at intervals ranging from 5-60 secs) and transient mode (data at 10-50Hz). When the pressure changes very quickly in a short time, the transient mode will be triggered. Each logger has a SIM card inside and an antenna outside to send data, which can be accessed online.
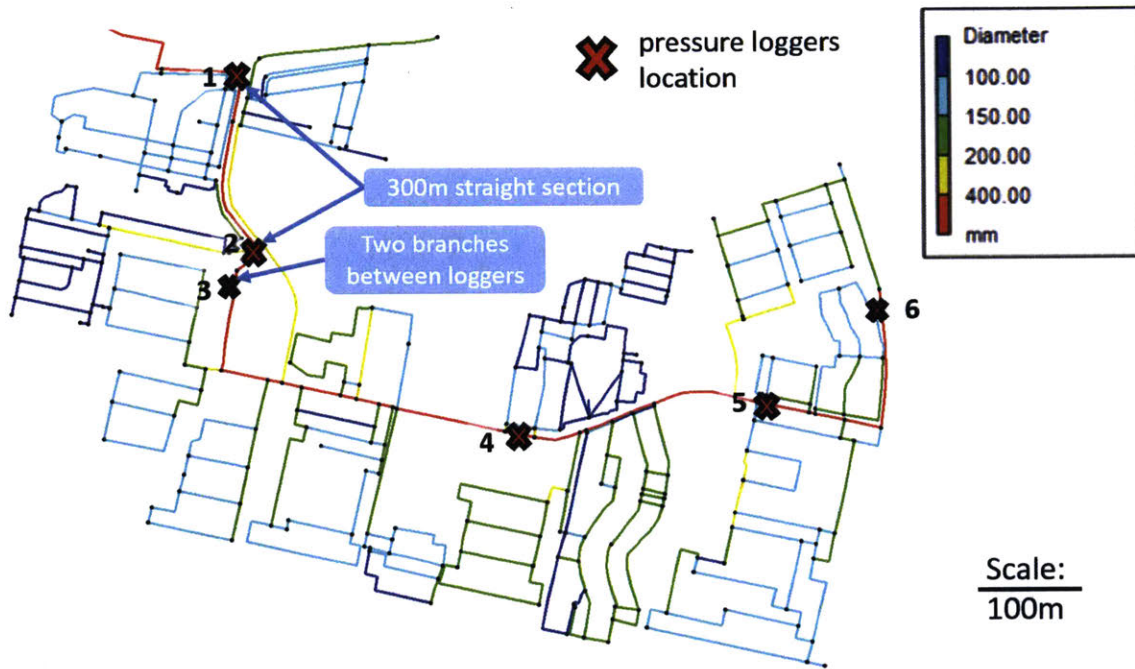
Figure 4-9: Field pipe network and pressure logger installations

A practical T junction is investigated in the field, and our model is used to run simulations and check if it can capture the real pressure changes at our measuring points. The geometry of the targeted field pipes is depicted in Figure 4-10. Numbers ranging from 0 to 8 in circles represent nodes, and numbers ranging from 0 to 7 represent pipes. Some other attributes are of pipes and nodes are described in Appendix B.

In the model, node 0 is the inlet node whose influx Q is set as $0.3m^3/s$ according to field data. Node 7 is a dead end, while node 6 and 8 are opened. The total simulation time is 1 hour with $dx = 1m$ and $dt = 0.015s$. Since specific data of all these branches or demand of necessary nodes are absent, orifice opening at node 6 and 8 are
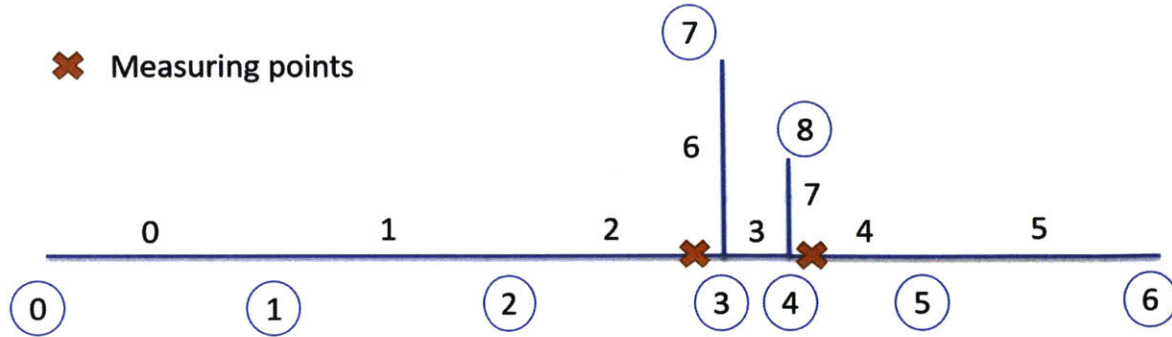
Figure 4-10: Simplified field pipe geometry for simulation

calibrated to help build water pressure in the trunk main. The comparison between numerical results and field data on 08/23/2016 is illustrated in Figure 4-11.

It can seen that our model can build pressure in a very short time with calibrated orifice openings, and the pressure generated by the model is in good agreement with the field data. Although there are still some divergences, it might be explained by the fact that the T junction in the field are not as perfect as what we have in the model. For example, the junction might be very old and or not correctly installed. It is also possible that the boundary conditions of the other nodes are not accurately characterized. Node 7 may not be a fully closed and there is still someone using the water from that pipe. If so, then the pressure after T can increase to be larger than the pressure before T. Moreover, it is noticeable that there is a short stage before the pressure reaches its steady peak. Although we use a different orifice opening to get our results, this phenomenon might result from the fact that pipe network grows like a tree, and some initial pressures are required to push the water into some branches and finally different households. This process takes some time and creates a steady pressure for a short period. After these branch pipes are full, the pipe pressure will continue to increase until the whole system reaches a steady state. More detailed information including the inlet pressure head and outflow distribution are presented in Appendix B.
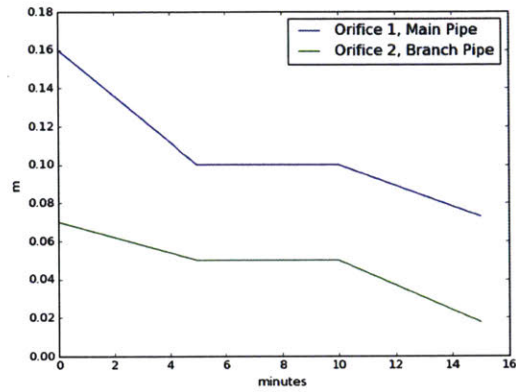
(a) Calibrated orifice opening for node 6(main) and 8(branch)
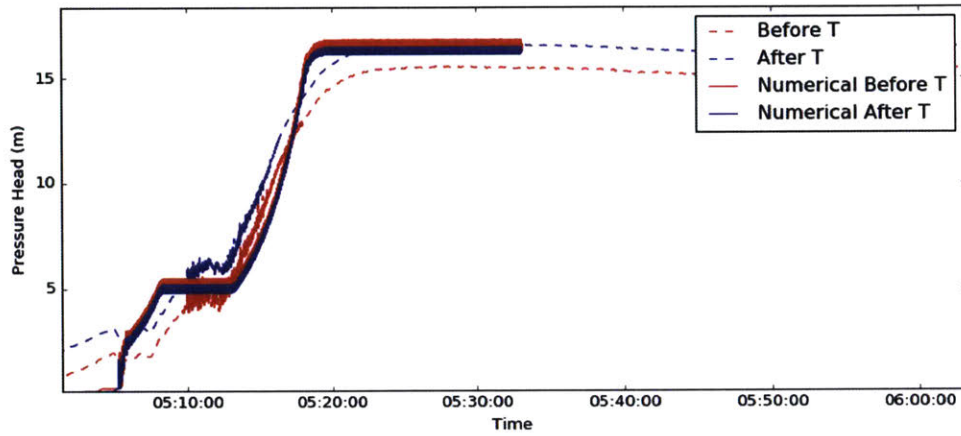
(b) Comparison between field data and numerical results

Figure 4-11: Field study and model calibration

4.5 Summary

This chapter presents several small-scale network examples built with the model. The first example is taken from a lab-scale experiment, and it is utilized to demonstrate that the model is able to solve the transient flow behavior with dry pipes. The second example is a single T junction with different initial conditions and boundary conditions to show that the model is able to process them. The third example is a H-shaped network including two T junctions, and its setup is more similar to the

network in the field. The fourth example is the field experiment conducted in Delhi, and the author went to the field to collect all the data required with the help of other researchers and field engineers. This field study is used to demonstrate that the model is capable of simulating the transient flow behavior in a real pipe network with T junctions.

Chapter 5

Simulation of A Large-Scale Network

In this chapter, the model is applied o simulate a large-scale network to capture the hydraulic dynamics of transient flow behavior. The whole network is shown in Figure 4-9 in Chapter 4. However, our model is not capable of simulating the network with loops yet, so those looped pipe subnetwork are replaced with a single pipe optimized to represent the same flow conditions. The new pipe network is a tree network, shown in Figure 5-1. There are many small black polygons in the figure representing the water demands of consumers, and the input boundary pressure is also presented for the specific node.

Input pressure boundary
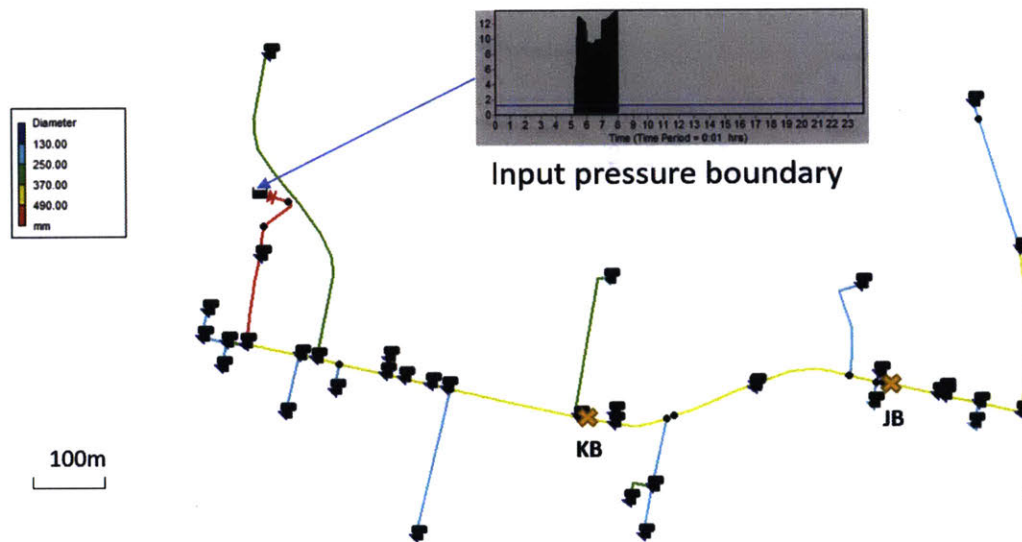
Figure 5-1: Modified Network of Figure 4-9

The network is composed of 98 pipes and 99 nodes, supplying water to around 40000 consumers. Two loggers from Telog, introduced in Chapter 4, are installed at the orange crosses. Their are referred to as KB and JB, respectively. The pressures at the boundary and the pressures measured by the two loggers for a single day are shown in Figure 5-2, and we scale the pressures during the water supply period, shown in Figure 5-3. These data provide benchmarks for our model calibrations.
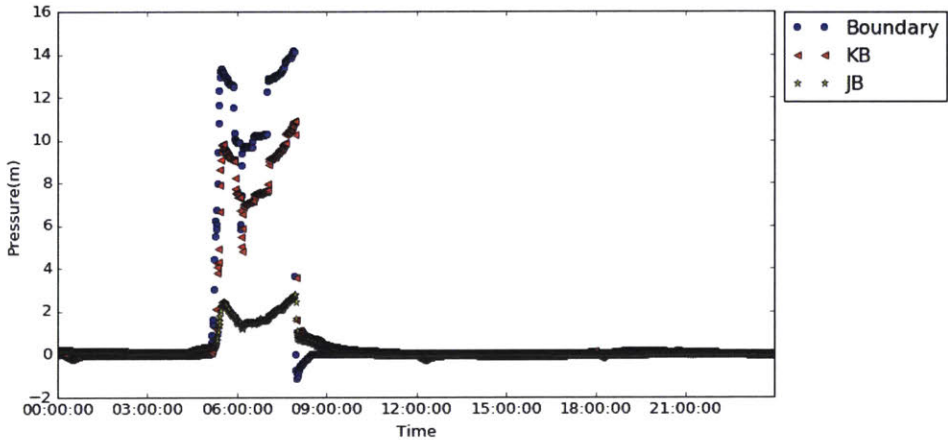
Figure 5-2: Pressures at the boundary and measured by two pressure loggers for a single day
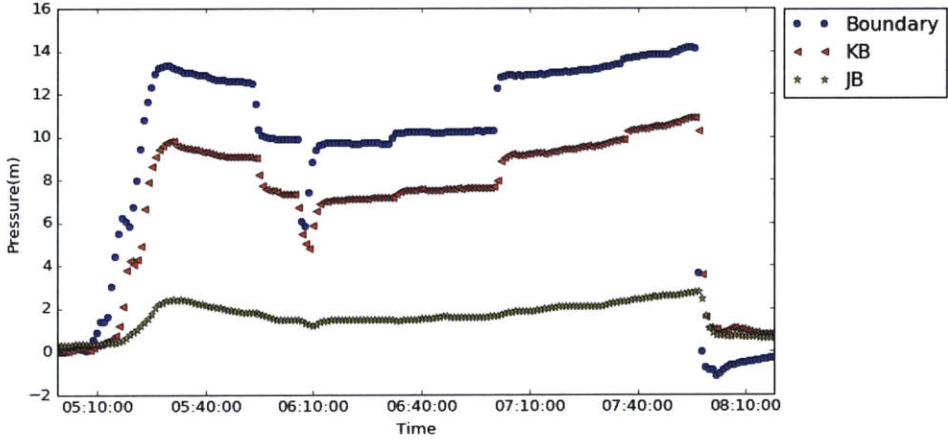
Figure 5-3: Pressures at the boundary and measured by two pressure loggers during the water supply period

The network can be simulated with EPANET, but the results are not in good agreement. By tuning parameters, a good match between the pressure data and the nu-

78

merical results from our model are achieved, shown in Figure 5-4. It can be seen that the field pressure can be successfully matched during the filling phase.
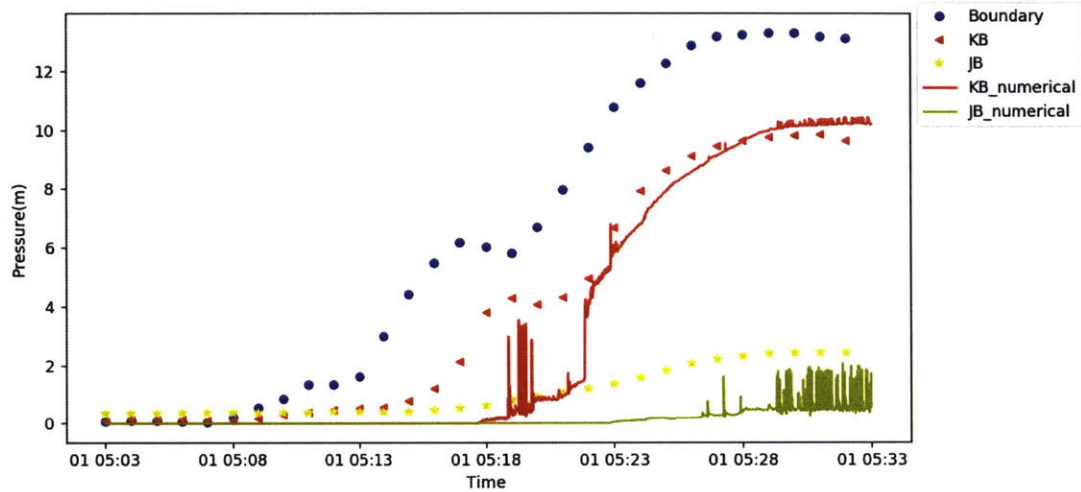
Figure 5-4: Comparison between the measured data and numerical results

There are some divergences at the beginning of filling period. It might because that the network is modified from the real network and the optimization process is only performed with EPANET using steady-state analysis. Therefore, the behavior of first several minutes are not fully captured.

Chapter 6

Summaries, Conclusions and Recommendations

6.1 Summaries

The thesis provides a basic description of IWS problems and illustrates the hydraulic model that is designed for the IWS system. In the first chapter, the universality and importance of IWS is emphasized and the negative influences on water quality and water distribution caused by IWS are further explained. Then difficulties that prevent the conversion of IWS to CWS are discussed, and the necessity of this thesis's work is stressed.

The second chapter states that the main challenge in modeling IWS is the transient flow modeling, which is controlled by the 1D Saint-Venant equations. Four numerical methods—the MOC, the shock capturing method, the PSM and the TPA method—used to solve the equations are reviewed and their advantages and disadvantages are discussed. Moreover, softwares that have been developed for modeling pipe networks are compared and shown in Table 2.1.

The third chapter describes the algorithm used in the model step by step. The general framework is taken from Lieb's work [43], and three parts are changed for

81

improvement: the calculation of the wave speed is modified to suppress the numerical oscillation [20]; the reconstruction algorithm is introduced to deal with dry pipes [77]; the three-pipe junction algorithm is developed to conserve mass, momentum and energy through the junction. Moreover, the three-pipe junction algorithm is validated with the data of local loss coefficients collected from previous papers. In addition, lessons from the author's hands-on experiences in using the model are provided to help users apply the model. Further, the influences of the wave speed are discussed and analyzed.

The fourth chapter shows several examples of small-scale networks that are built with the model. A lab-scale experiment is presented to demonstrate the model's ability to handle dry pipes. Other examples of T junctions, including a field study in India, are provided to argue that the model is able to correctly process T junction. In addition, some divergences between the modeling results and measured data are discussed and reasonably explained.

The fifth chapter is the application of the model in a large-scale network. By comparing with the steady state results from EPANET, It suggests the model's applicability in the field and provides more information about the transient flow behavior of IWS in the real world.

6.2   Conclusions

Although no water supply pipe networks are initially built to serve water intermittently, many reasons, such as limited water resources and serious leakages, cause the Intermittent water supply (IWS) to be widespread in the world [69, 2]. IWS not only makes people's life inconvenient, but also has serious negative effects on the water quality and thus is harmful to people's health. It is a disturbing problem that many engineers and researchers are struggling to solve, and international agencies are making efforts to convert the IWS systems to continuous water supply (CWS) systems

[54]. However, the conversion is a very slow process and more than half people in Asia are still suffering from the problems brought by IWS [67]. Some countries, like India, have enough water but the old pipe networks have so many unknown leakages that the huge water loss from these leakages, sometimes can be as high as 45%, prevent them from achieving CWS [75]. It is unrealistic to replace all old pipes with new ones, but finding those leakages to fix them can help achieve a low-cost conversion from IWS to CWS. Having a model that is able to simulate the transient flow behavior in the IWS system can help us understand the pressure changes during the entire supply period, and it is very helpful to locate leakages with pressure signals in the future.

The main difficulty of modeling IWS resides in the modeling of the transient flow governed by the 1D Sanit-Venant equations. Four methods have been developed in the past several decades to help solve these equations. The MOC is very flexible to solve the water channels with complex geometries, but it is mostly applied to rivers and cannot solve the situation that the open channel flow and pressurized flow coexist in the same pipe. The shock capturing method is developed based on MOC, but the interface between the open channel flow and pressurized flow needs to be guessed when the pipe is empty. Both the PSM and the TPA method assume a small slot on the pipe crown and thus only the open channel equations need to be solved. These two methods are also becoming increasingly popular these days.

The numerical algorithm we use for IWS is initially built by Dr. Anna Lieb in UC Berkeley, and we make modifications to further improve it. The comparison among the improved model and other softwares are shown in Table 6.1. Results suggest that our three-pipe junction algorithm is able to match the local loss coefficients reported by many researchers in experiments, and those examples of small-scale networks demonstrate that the improved model can correctly reproduce the results of transient flow in dry pipes and the pipe network with T junctions with tolerable errors. Moreover, the simulation of a large-scale network helps the understanding of the hydraulic dynamics of IWS in the real world.

Table 6.1: Comparison among different softwares modeling the transient flow in pipe networks (including the improved model)

Software	SWMM	ITM	Software by Dr. Lieb	Improved Model
Dry pipes	✓	✓	✗	✓
Two-pipe junctions	✓	✓	✓	✓
Three-pipe junctions (mass conservation)	✓	✓	✓	✓
Three-pipe junctions (momentum conservation)	✓	✓	✗	✓
Three-pipe junctions (energy conservation)	✓*	✓*	✗	✓
Looped network	✓	✓	✗	✗
Water hammer effects	✗	✓	✓	✓
Subatmospheric pressure	✗	✓	✗	✗
Air pockets	✗	✗	✗	✗
Numerical Oscillation	✓	✓	✗	✓
Short simulation time	✓	✗	✓	✓
Friendly user interface	✓	✓	✗	✗
Readily amendable	✗	✗	✓	✓

* requires manual calibration

6.3 Recommendations

Although we have improved the numerical model to account for the situation with dry pipes and three-pipe junctions, there are still some limitations. The most urgent one is that the algorithm for two scenarios at the T junction, shown in Figure 6-1, have not been developed yet. Without this algorithm, the model cannot be applied to a looped network. Moreover, the PSM cannot simulate the subatmospheric pressure in

the pipe, which can happen when no ventilation is available. The TPA method might be a solution, but it may require more efforts to reframe the model. Further, the air pocket effects, which can cause oscillating pressure known as Helmholtz instability, may need to be taken into consideration in the future.

(a) Combining flow, outflow from the branch pipe

(b) Dividing flow, inflow from the branch pipe
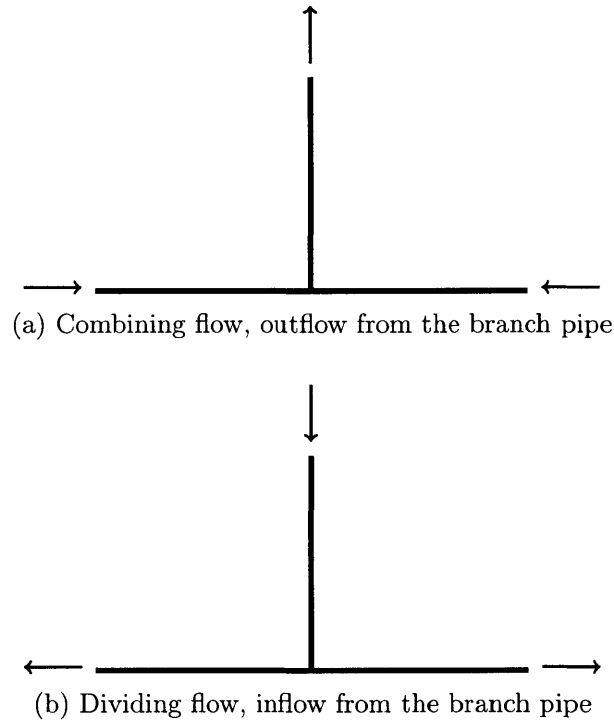
Figure 6-1: Two missing scenarios at the T junction

It should also be noticed that the field is much more complicated that expected, especially when compared with the laboratory setup. For example, actual pipe's roughness is not only decided by the material, but also influenced by the time that the pipe has been used and the surrounding environment that the pipe is installed. For example, a CI pipe has been used for 20 years should have a different roughness from a CI pipe that has been used for 5 years, and a CI pipe that has been put underground for 20 years can have a significantly different roughness from a CI pipe that has been exposed to the atmosphere on the ground for 20 years. Even all these factors are the same, a CI pipe that has water in it 3 hours a day can have a different roughness from a CI pipe that has water in it 10 hours a day due to different erosions. Therefore, estimation of the roughness can be a very important process

before modeling. Moreover, there are several terrible facts that increase the difficulty of applicable research. For example, it is found that sometimes small pipes, instead of using a T junction, are directly inserted into a large pipe, which causes unpredicted minor loss that no one has measured before. Furthermore, the pipe network shown on the map may not be exactly the same as the real layout of the network in the field, and this requires researchers to conduct the field study very carefully. If a user find his model's results are different from the field data, the reliability of input parameters should also be a concern.

Appendix A

Influences of Air on Wave Velocity

The expression of bulk modulus is

$$K = -V \frac{dp}{dV}. \tag{A.1}$$

With entrapped air, the expression is written as

$$\frac{K^*}{K} = \frac{1 + \frac{V_{air}}{V_{fluid}}}{1 + \frac{p_0 V_{air}}{p V_{fluid}} \frac{K}{p}} = \frac{1}{1 + \frac{V_{air}}{V_{total}} \frac{K}{p}}, \tag{A.2}$$

where K^* is the new modulus, V_{air} and V_{fluid} denotes the volume of air and fluid, respectively. p_0 is the air pressure in the pipe and p is the fluid pressure. For water,

$$K = 2.15 \times 10^9 Pa.N/m^2.$$

When $T = 21^\circ C$,

$$E_{steel} = 2.0 \times 10^{11} Pa,$$

$$E_{grayCI} = 9.24 \times 10^{10} Pa,$$

$$E_{ABSplastics} = 1.4 - 3.1 \times 10^9 Pa.$$

Assuming a pipe whose outside diameter is 24 inches with 1 inch thickness, the influences of air on wave velocity is shown in Figure A-1.
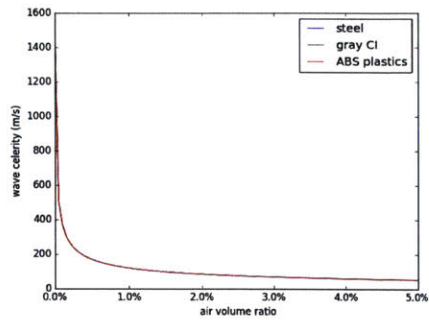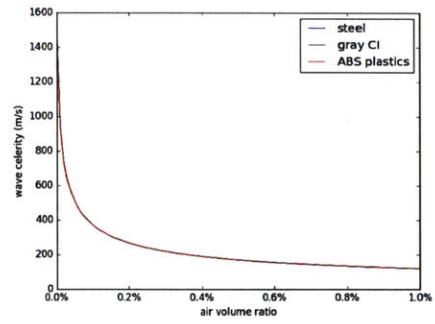
(a)   (b)

Figure A-1: The relationship between entrapped air volume and wave velocity. (a) is the main plot, and (b) scales part of (a)

Appendix B

Field Study Detailed Information

Table B.1: Attributes of pipes 0-7

Pipe	Inlet Node	Outlet Node	$L(m)$	$D(m)$	Mn
0	0	1	208	0.6	0.013
1	1	2	230	0.6	0.013
2	2	3	54	0.6	0.013
3	3	4	8	0.6	0.012
4	4	5	35	0.6	0.013
5	5	6	123	0.6	0.013
6	3	7	285	0.25	0.013
7	4	8	100	0.3	0.013

Table B.2: Elevations of Nodes 0-8

Node	Elevation (m)
0	232.00
1	233.65
2	233.90
3	234.00
4	234.20
5	233.20
6	233.00
7	233.50
8	233.60
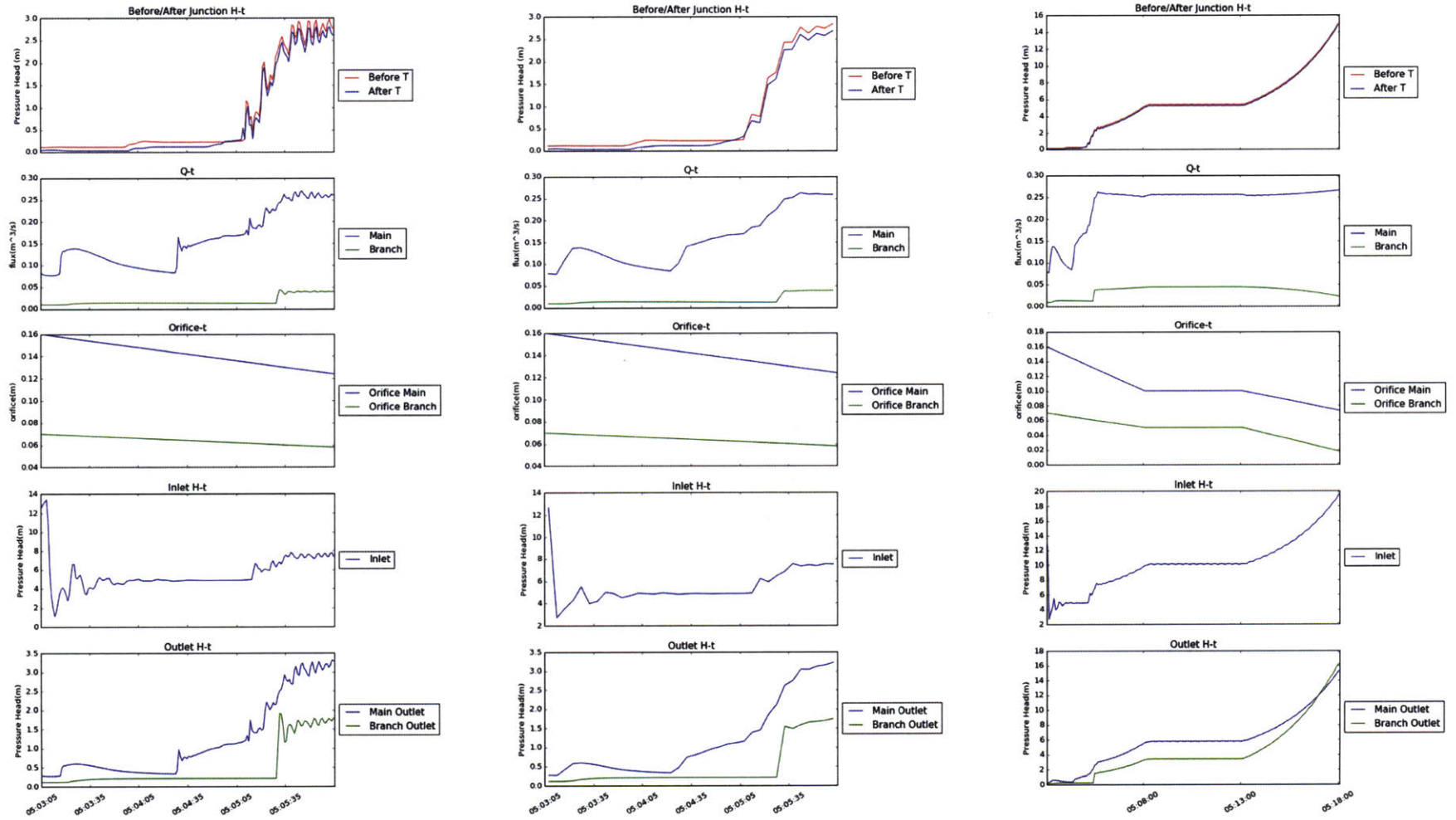
(a) First 3 minutes, averaged over 1 second (b) First 3 minutes, averaged over 5 seconds (c) First 15 minutes, averaged over 5 seconds

Figure B-1: Numerical simulation results for field study

Bibliography

[1] Carpenter, A. The fever at croydon: And intermittent water-supply as a cause of typhoid. *British medical journal*, 2(777):632, 1875.

[2] Franceys, R., & Jalakam, A. The karnataka urban water sector improvement project; 24x7 water supply is achievable. *Water and Sanitation Program, The World Bank, Tech. Rep*, 2010.

[3] Gardal, A. Losses of load in flowers through branch teams. *Lausanne Univ. Polytech. Ecole Pub*, 50:1–13, 1957.

[4] Gardel, A. Pressure drops in flows through t-shaped fittings. *Bulletin technique de la Suisse Romande*, 9:123–130, 1957.

[5] Ingeduld, P., Pradhan, A., Svitak, Z., & Terrai, A. Modelling intermittent water supply systems with EPANET. In *Water Distribution Systems Analysis Symposium 2006*, pages 1–8, 2008.

[6] Preissmann, A. Propagation des intumescences dans les canaux et rivieres. In *First Congress French Assoc. for Computation*, 1961.

[7] Trajkovic, B., Ivetic, M., Calomino, F., & DIppolito, A. Investigation of transition from free surface to pressurized flow in a circular pipe. *Water science and technology*, 39(9):105–112, 1999.

[8] Vacs R., & Deborah A. *The effects of an intermittent piped water network and storage practices on household water quality in Tamale, Ghana.* PhD thesis, Massachusetts Institute of Technology, 2013.

[9] McIntosh, A.C. *Asian water supplies reaching the urban poor.* Asian Development Bank, 2003.

[10] Eichenwald, Z., & McGarity, A.E. Watershed-based optimal stormwater management: Part 2 -hydrologic modeling of lid/bmp sites on little crum creek in suburban philadelphia. In *World Environmental and Water Resources Congress 2010: Challenges of Change*, pages 2522–2530, 2010.

[11] Wisner, P.E., Roake, A.F., & Ashamalla, A.F. Application of storm and swmm for assessment of urban drainage alternatives in canada. 1976.

[12] Srirangarajan, S., Allen,M., Preis,A., Iqbal,M., Lim, H.B., & Whittle, A.J. Wavelet-based burst event detection and localization in water distribution systems. *Journal of Signal Processing Systems*, 72(1):1–16, 2013.

[13] S.P., & Kelkar, P.S. Andey. Performance of water distribution systems during intermittent versus continuous water supply. *Journal (American Water Works Association)*, 99(8):99–106, 2007.

[14] Leon, A.S. *Improved modeling of unsteady free surface, pressurized and mixed flows in storm-sewer systems*, Volume 68. 2007.

[15] Mermin, J. H., Villar, R., Carpenter, J., Roberts, L., Samaridden, A., Gasanova, L., ... & Ross, B. A massive epidemic of multidrug-resistant typhoid fever in tajikistan associated with consumption of municipal water. *Journal of Infectious Diseases*, 179(6):1416–1422, 1999.

[16] Nesbitt, B. *Handbook of pumps and pumping: Pumping manual international.* Elsevier, 2006.

[17] R.A. Bajura. A model for flow distribution in manifolds. *Journal of Engineering for power*, 93(1):7–12, 1971.

[18] Begnudelli, L., & Sanders, B.F. Unstructured grid finite-volume algorithm for shallow-water flow and scalar transport with wetting and drying. *Journal of Hydraulic Engineering*, 132(4):371–384, 2006.

[19] Begnudelli, L., & Sanders, B.F. Simulation of the st. francis dam-break flood. *Journal of Engineering Mechanics*, 133(11):1200–1212, 2007.

[20] Malekpour, A., & Karney, B.W. Spurious numerical oscillations in the preissmann slot method: Origin and suppression. *Journal of Hydraulic Engineering*, page 04015060, 2015.

[21] Constantin, P., & Foias, C. *Navier-stokes equations.* University of Chicago Press, 1988.

[22] Gottlieb, S., & Shu, C. Total variation diminishing runge-kutta schemes. *Mathematics of computation of the American Mathematical Society*, 67(221):73–85, 1998.

[23] James, W., Rossman, L. A., & James, W. R. C. User's guide to swmm 5:[based on original usepa swmm documentation]. CHI, 2010.

[24] Semenza, J.C., Roberts, L., Henderson, A., Bogan, J., & Rubin, C.H. Water distribution system and diarrheal disease transmission: a case study in uzbekistan. *The American Journal of Tropical Medicine and Hygiene*, 59(6):941–946, 1998.

[25] Wiggert, D.C. Transient flow in free-surface, pressurized systems. *Journal of the Hydraulics division*, 98(1):11–27, 1972.

[26] Mitchell, A.R., & Griffiths, D.F. *The finite difference method in partial differential equations*. John Wiley, 1980.

[27] George, D.L. *Numerical approximation of the nonlinear shallow water equations with topography and dry beds: A Godunov-type scheme*. PhD thesis, University of Washington, 2004.

[28] Margaris, D.P. T-junction separation modelling in gas–liquid two-phase flow. *Chemical Engineering and Processing: Process Intensification*, 46(2):150–158, 2007.

[29] Miller, D.S. Internal flow: a guide to losses in pipe and duct systems. In *Internal flow: a guide to losses in pipe and duct systems*. British Hydromechanics Research Association, 1971.

[30] Miller, D.S. *Internal flow system*. BHRA, 1990.

[31] Kinne, E. Contribution to the knowledge of hydraulic losses in branches. *Mitteilungen, Hydraulischen Institute*, pages 70–93, 1931.

[32] Swerdlow, D. L., Greene, K. D., Tauxe, R. V., Wells, J. G., Bean, N. H., Ries, A. A., ... & Tejada, E. Waterborne transmission of epidemic cholera in trujillo, peru: lessons for a continent at risk. *The Lancet*, 340(8810):28–32, 1992.

[33] Toro, E.F. *Riemann solvers and numerical methods for fluid dynamics: a practical introduction*. Springer Science & Business Media, 2013.

[34] Carter, C. S., Byun, S. A., & Marengo, B. G. Evaluation of inflatable dams for in-system storage utilization in cso abatement. In *Urban Drainage Modeling*, pages 110–122. 2001.

[35] Dhatt, G., LefranÃğois, E., & Touzot, G. *Finite element method*. John Wiley & Sons, 2012.

[36] Vogel, G. Investigation of the loss in right-angled pipe branches. *Mitt. Hydraulischen Instituts der Tech. Hoschul. Munchen*, (1):75–90, 1926.

[37] Yao, C., Dong, Z., Zhao, Y., & Chen, G. Gas-liquid flow and mass transfer in a microchannel under elevated pressures. *Chemical Engineering Science*, 123:137–145, 2015.

[38] Courant, R., Friedrichs, K., & Lewy, H. On the partial difference equations of mathematical physics. *IBM journal*, 11(2):215–234, 1967.

[39] LeÃşn, A. S., Ghidaoui, M. S., Schmidt, A. R., & GarcÃŋa, M. H. Godunov-type solutions for transient flows in sewers. *Journal of Hydraulic Engineering*, 132(8):800–813, 2006.

[40] Yamaguchi, H. *Engineering fluid mechanics*, Volume 85. Springer Science & Business Media, 2008.

[41] Butcher, J. Runge-kutta methods. *Scholarpedia*, 2(9):3147, 2007.

[42] Howard, G., & Bartram, J. Domestic water quantity. *Service level and health*, 2003.

[43] Lieb, A.M., Rycroft, C.H., & Wilkening, J. Optimizing intermittent water supply in urban pipe distribution networks. *arXiv preprint arXiv:1509.03024*, 2015.

[44] Preis, A., Allen, M., & Whittle, A. J. On-line hydraulic modeling of a water distribution system in singapore. In *Water Distribution Systems Analysis 2010*, pages 1336–1348. 2010.

[45] Cunge, J.A. Discussion of "Transient Mixed-Flow Models for Storm Sewers". *Journal of Hydraulic Engineering*, 111(3):557–559, 1985.

[46] Song, C., Gavali, S., & Cardle, J.A. Mathematical modeling of the genesee river storage-conveyance system rochester, new york. 1982.

[47] Anderson, J.D. and Wendt, J. *Computational fluid dynamics*, Volume 206. Springer, 1995.

[48] McNown, J.S. Mechanics of manifold flow. *Transactions of the American Society of Civil Engineers*, 119(1):1103–1118, 1954.

[49] Itō, H., & Imai, K. Energy losses at 90 pipe junctions. *Journal of the Hydraulics Division*, 99(9):1353–1368, 1973.

[50] Sashikumar, N., Mohankumar, M. S., & Sridharan, K. Modelling an intermittent water supply. In *World Water & Environmental Resources Congress 2003*, pages 1–11, 2003.

[51] Bathe, K.J. *Finite element method*. Wiley Online Library, 2008.

[52] Lee, E.J., & Schwab, K.J. Deficiencies in drinking water distribution systems in developing countries. *Journal of water and health*, 3(2):109–127, 2005.

[53] Kumpel, E., & Nelson, K.L. Comparing microbial water quality in an intermittent and continuous piped water supply. *Water research*, 47(14):5176–5188, 2013.

[54] Kumpel, E., & Nelson, K.L. Intermittent water supply: prevalence, practice, and microbial water quality. *Environmental science & technology*, 50(2):542–553, 2016.

[55] Song, Charles, C.S., Cardie, J.A., & Leung, K.S. Transient mixed-flow models for storm sewers. *Journal of hydraulic engineering*, 109(11):1487–1504, 1983.

[56] Kumpel, E., & Nelson, K. L. Mechanisms affecting water quality in an intermittent piped water supply. *Environmental science & technology*, 48(5):2766–2775, 2014.

[57] Rossman, L.A. Computer models/ EPANET. *Water distribution systems handbook, New York: McGraw Hill*, 1999.

[58] Rossman, L.A. Epanet 2: users manual. 2000.

[59] R., Cawley, P., & Lowe, M. Long. Acoustic wave propagation in buried iron water pipes. In *Proceedings of the Royal Society of London A: Mathematical, Physical and Engineering Sciences*, Volume 459, pages 2749–2770. The Royal Society, 2003.

[60] Cunge, J.A., & Wegner, M. Intégration numérique des équations d'écoulement de barré de saint-venant par un schéma implicite de différences finies. *La Houille Blanche*, (1):33–39, 1964.

[61] Ercumen, A., Arnold, B. F., Kumpel, E., Burt, Z., Ray, I., Nelson, K., & Colford Jr, J. M. Upgrading a piped water supply from intermittent to continuous delivery and association with waterborne illness: a matched cohort study in urban india. *PLoS medicine*, 12(10):e1001892, 2015.

[62] Lister, M. The numerical solution of hyperbolic partial differential equations by the method of characteristics. *Mathematical methods for digital computers*, 1:165–179, 1960.

[63] Abbott, M.B. An introduction to the method of characteristics. 1966.

[64] León, A.S, Ghidaoui, M.S., Schmidt, A.R., & García, M.H. Application of godunov-type schemes to transient mixed flows. *Journal of hydraulic research*, 47(2):147–156, 2009.

[65] LeÃşn, A.S., Liu, X., Ghidaoui, M.S., Schmidt, A.R., & GarcÃŋa, M.H. Junction and drop-shaft boundary conditions for modeling free-surface, pressurized, and mixed free-surface pressurized transient flows. *Journal of Hydraulic Engineering*, 136(10):705–715, 2010.

[66] Abou-Haidar, N.I. *Compressible flow pressure losses in branched ducts*. PhD thesis, University of Liverpool, 1989.

[67] World Health Organization et al. *Global water supply and sanitation assessment 2000 Report*. World Health Organization, 2000.

[68] Aureli, F., Dazzi, S., Maranzoni, A., & Mignosa, P. Validation of single-and two-equation models for transient mixed flows: a laboratory test case. *Journal of Hydraulic Research*, 53(4):440–451, 2015.

[69] Klingel, P. Technical causes and impacts of intermittent water distribution. *Water Science and Technology: Water Supply*, 12(4):504–512, 2012.

[70] Azzopardi, B.T., & Whalley, P.B. The effect of flow patterns on two-phase flow in a t junction. *International Journal of Multiphase Flow*, 8(5):491–507, 1982.

[71] Roache, P.J. Fundamentals of computational fluid dynamics(book). *Albuquerque, NM: Hermosa Publishers, 1998.*, 1998.

[72] Vasconcelos, J.G., Wright, S.J., & Roe, P.L. Improved simulation of flow regime transition in sewers: Two-component pressure approach. *Journal of Hydraulic Engineering*, 132(6):553–562, 2006.

[73] Blaisdell, F.W., & Manson, P.W. *Loss of energy at sharp-edged pipe junctions in water conveyance systems*, Volume 1281. Agricultural Research Service, US Department of Agriculture, 1963.

[74] Dasgupta, P., & Dasgupta, R. Economic value of safe water for the infrastructurally disadvantaged urban household: A case study in delhi, india. *Water resources research*, 40(11), 2004.

[75] Batish, Rajiv. A new approach to the design of intermittent water supply networks. In *World Water & Environmental Resources Congress*, pages 1–11, 2003.

[76] LeVeque, R.J. *Finite volume methods for hyperbolic problems*, Volume 31. Cambridge university press, 2002.

[77] Sanders, B.F., & Bradford, S.F. Network implementation of the two-component pressure approach for transient flow in storm sewers. *Journal of hydraulic engineering*, 137(2):158–172, 2010.

[78] Chen, S.H. Finite difference method. *High-Field Physics and Ultrafast Technology Laboratory, Taipei, Taiwan*, 2006.

[79] Vasconcelos, J.G., & Wright, S.J. Comparison between the two-component pressure approach and current transient flow solvers. *Journal of Hydraulic Research*, 45(2):178–187, 2007.

[80] Abou-Haidar, N.I., & Dixon, S.L. Compressible flow losses in branched ducts. In *Heat Transfer 1988*, Volume 2, pages 17–23, 1988.

[81] Abou-Haidar, N.I., & Dixon, S.L. Pressure losses in combining subsonic flows through branched ducts. In *ASME 1990 International Gas Turbine and Aero-engine Congress and Exposition*, pages V001T01A041–V001T01A041. American Society of Mechanical Engineers, 1990.

[82] Wylie, E.B., & Streeter, V.L. Fluid transients. *New York, McGraw-Hill International Book Co., 1978. 401 p.*, 1, 1978.

[83] Hunaidi, O., & Chu, W.T. Acoustical characteristics of leak signals in plastic water distribution pipes. *Applied Acoustics*, 58(3):235–254, 1999.

[84] Capart, H., Eldho, T.I., Huang, S.Y., Young, D.L., & Zech, Y. Treatment of natural geometry in finite volume river flow computations. *Journal of Hydraulic Engineering*, 129(5):385–393, 2003.